

# The Geomorphology and Evolution of Hecate Chasma, Venus

VICTORIA E. HAMILTON

*Department of Geology, Arizona State University, Tempe, Arizona 85287*  
E-mail: hamilton@esther.la.asu.edu

AND

ELLEN R. STOFAN

*Jet Propulsion Laboratory, California Institute of Technology, Pasadena, California 91109*

Received May 11, 1995; revised October 26, 1995

---

Hecate Chasma is a discontinuous trough and fracture system extending from Atla Regio through Asteria Regio. A detailed examination of Hecate Chasma using Magellan image and altimetry data reveals morphologic features such as normal faults (including graben), compressional ridges, a variety of volcanic edifices, and coronae. There is no evidence for a systematic age progression among coronae in chains, thus a single, stationary thermal anomaly underlying a moving lithosphere is an unlikely origin for the chains. A comparison of the observed features with two possible models of evolution, subduction/delamination or lithospheric extension with limited rifting, shows some similarities between the predicted morphologies of each model and Hecate Chasma. The dominance of features related to upwelling and extensional tectonism strongly favor an extensional origin for this zone. The corona chain may have been formed by upwellings related to Rayleigh–Taylor instabilities, similar to those observed at terrestrial mid-ocean ridges, but in an environment of limited spreading. © 1996

Academic Press, Inc.

---

## INTRODUCTION

In the absence of Earth-like plate tectonics, global heat loss on Venus has been attributed to a combination of lithospheric recycling, conduction/thermal thinning, and volcanism (Solomon and Head 1982), with conduction dominating global heat loss (Grimm and Solomon 1987). Surface manifestations of mantle upwelling may range from clusters of small volcanoes (<30 km diameter) to major volcanic rises and coronae (Masursky *et al.* 1980, McGill *et al.* 1981, Barsukov *et al.* 1986, Stofan and Head 1990, Head *et al.* 1992, Stofan *et al.* 1992). The high resolution Magellan data set has allowed for a detailed study of these surface expressions of mantle activity, as well as their local and regional geological settings.

Coronae are of particular interest because their depths of origin and evolution are less clearly understood than those of the major volcanic centers. Understanding the local distributions of coronae, their morphologies, and associated tectonics in regions of high corona population will help provide additional constraints on venusian interior processes. In planform, coronae are large circular to elliptical features which range in size from 60 to over 900 km in diameter and display a multitude of tectonic features indicative of extension, compression, or both (Stofan *et al.* 1992). The spatial occurrence of coronae, ranging from solitary to clusters to chains, is of interest in understanding their relation to mantle processes. The typical topography and tectonic and volcanic characteristics of coronae support a model of formation by mantle upwelling or mantle diapirs (Stofan and Head 1990, Pronin and Stofan 1990, Schubert *et al.* 1990, Stofan *et al.* 1987, 1991, 1992, Squyres *et al.* 1992, Janes *et al.* 1992). Squyres *et al.* (1993) found that coronae are preferentially located at elevations near mean planetary radius (MPR), and that the only statistically significant clustering of coronae is near the equator in the Beta-Atla-Themis (BAT) region, which includes the corona chain along Hecate Chasma. The BAT region is believed to be a zone of broad-scale mantle upwelling that produces a higher concentration of smaller-scale diapirs (Squyres *et al.* 1993). This broad zone of deformation and enhanced diapirism may be an important contributor to global heat loss if accompanied by significant lithospheric thinning and enhanced conductive heat loss. Coronae concentrated in chains do not consistently display any clear age progression or systematic variation in topography or morphology, and are therefore not believed to be indicative of a thermal anomaly characterized by a singular source underlying a moving lithosphere (Stofan *et al.* 1992). The small size of the majority of coronae in com-

parison to terrestrial hotspots may indicate shallower depths of origination for corona-forming diapirs as discussed below.

This paper focuses on the corona chain and accompanying deformational zone in Hecate Chasma. First we describe the characteristic structures, volcanic features, and coronae found along Hecate Chasma, and then we review the geomorphology along the strike of the deformational zone. Based on the geologic observations, two possible modes of evolution for the development of Hecate Chasma are discussed: subduction/delamination (Sandwell and Schubert 1992a, 1992b), or extension accompanied by limited rifting (Hamilton and Stofan 1993, 1994; Stofan *et al.* 1993).

## GEOLOGICAL FEATURES OF HECATE CHASMA

### *General Description*

Hecate Chasma (Fig. 1) is a fracture belt over 8000 km in length with a discontinuous trough and associated corona chain located at the eastern end of Aphrodite Terra between 203°E and 278°E longitude and ranging from 10°S to 30°N latitude. The corona chain and chasm exhibit en echelon offsets along strike, but follow an overall WSW–ENE trend from Atla Regio to Beta Regio. As a result of the dense spacing of fractures along strike, the bounding fractures of the trough are very difficult to discern from Magellan SAR images alone. Plains units surrounding Hecate Chasma lie approximately 0.5 km above MPR and appear to be mostly radar-dark plains and mottled plains which are interpreted to be volcanic flood plains (e.g., Roberts *et al.* 1992, Head *et al.* 1992).

Magellan altimetry over the Hecate Chasma region show general correlations with geologic features. Topography for the main Hecate Chasma region is shown in Fig. 2. The coronae and fracture belt lie along a regional rise which averages 0.5–1.0 km in elevation above the surrounding plains. The deepest segments of the chasm, located in east-central Hecate, reach 3–4 km below MPR in places, and the rims of the trough are as high as 3–4 km in elevation; the net difference in some places yields a trough with up to 6 km of relief over a horizontal distance of a few tens of kilometers. The trough segments are generally correlated to the most concentrated areas of fracturing (Fig. 3).

An examination of the emissivity, slope roughness (RMS), and reflectivity data in the vicinity of Hecate Chasma established that this region has average values similar to the planetary averages. As these data do not display any unusual trends that cannot easily be explained by the local geology, they were of limited use in this study.

### *Morphologic Settings*

Hecate Chasma is characterized by two gradational but distinct morphologies, both associated with coronae: a re-

gion of diffuse fracturing with minor chasm development (Fig. 4a), and a region of dense fracturing with significant trough development (Fig. 4b). We will refer to the first type as a diffuse fracturing morphology and the second as a trough-dominated morphology.

Diffusely fractured regions tend to be dominated by graben and lineaments of indeterminate origin with intermittently spaced coronae. Coronae in these zones typically have extensive volcanism associated with them, are defined by topographic plateaus, and have sub-radial graben in their interiors. These zones are interpreted to be accommodating tectonism broadly rather than in narrow regions of localized deformation.

Zones with trough-dominated morphologies have highly concentrated fractures, which are distinguishable as normal faults and normal faults defining graben sets. These zones are typified by extensive digitate lava flows and have deep troughs parallel to the trend of faulting. Coronae along these sections commonly have well-defined annuli, raised rims, and central depressions, and radial lineaments are less pervasive. Additionally, these coronae are located immediately adjacent to the deep troughs.

These two morphologic terrains appear to represent two different modes of accommodating tectonism, one broad and the other more localized. It may be that these areas represent stages in the tectonic evolution of the zone, a possibility which will be discussed later in this paper.

### *Geologic Features*

*Structural features.* Complex and linear deformation patterns define the Hecate Chasma region. Linear structures typically follow the WSW–ENE trend of the chasm, but may locally trend more to the SW–NE or W–E along en echelon offsets. Fracture density decreases dramatically about 150–200 km away from the trough and coronae. At the far eastern end of Hecate, in Asteria Regio, the path of the fracture system bifurcates, with one arm trending to the NE and the other arm more easterly (Fig. 3). Terrain with complex patterns termed tessera (or complex ridged terrain) is uncommon along Hecate Chasma and occurs only at the eastern end of the chasm near Beta Regio. Tessera is interpreted to be the oldest terrain in the region (Senske *et al.* 1991a, 1991b).

Linear features are the dominant structures defining Hecate Chasma. Lineaments are recognizable by their radar-brightness and straight or slightly sinuous trends. Linear features display two wavelengths of deformation, one wavelength defined by the trough width (100–200 km), and the other by structures within the chasma region (~2–30 km). Although the Hecate Chasma deformational zone generally trends WSW–ENE, the short wavelength linear fractures trend primarily W–E or SW–NE, parallel to the trough, and are generally located within about 400



FIG. 1. Magellan radar image of Hecate Chasma. Latitude 8°S to 30°N, longitude 199.5°E to 278°E. Scale: 1 cm = 335 km. Portion of MRPS 43327.

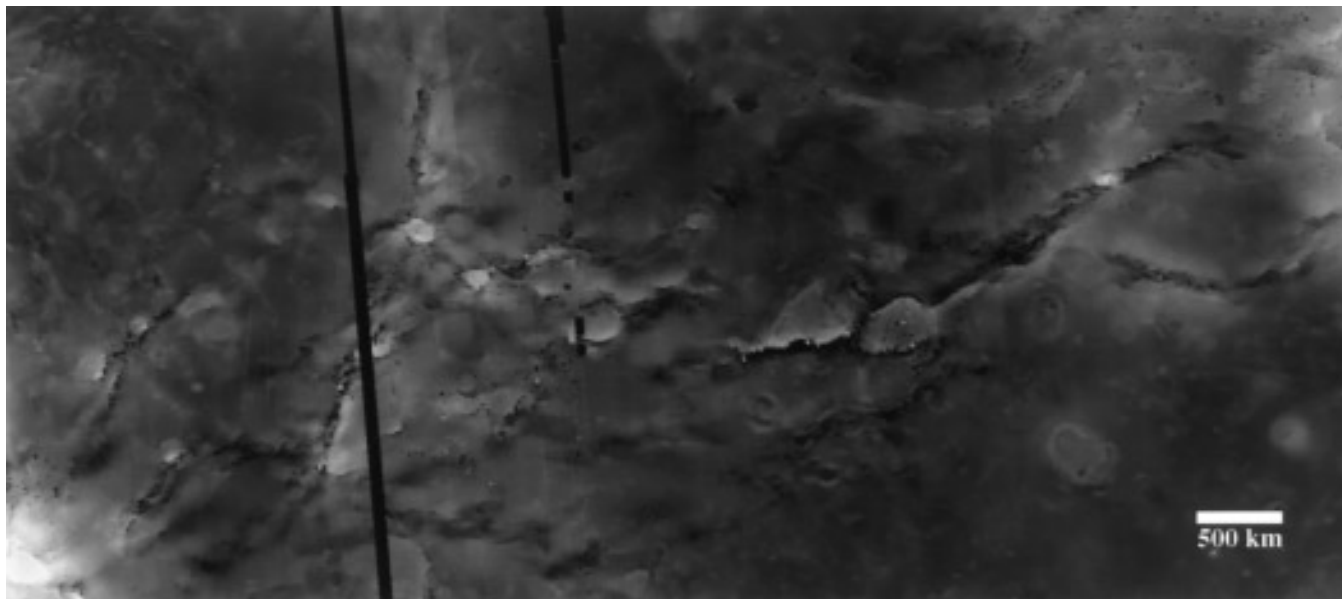


FIG. 2. Topography of Hecate Chasma. Latitude 0.5°N to 33.7°N, longitude 199.5°E to 278°E. Elevation ranges from 6047.9 to 6058.7 km.

km of the trough, indicating that they are related to trough-forming processes. Faint lineament sets crossing at 60° angles (trending WNW and ENE) are commonly seen in the relatively undeformed plains units surrounding Hecate Chasma. Lineaments also connect the coronae associated with Hecate Chasma, and in many cases merge with the annular fractures defining a corona. Many lineaments are directly related to corona features, either forming the annuli or the radial fractures in the corona interiors. The fractures defining the annuli are typically extensional and, more rarely, compressional in origin, and radial interior fractures are generally graben as expected according to the global characteristics of coronae and models of corona formation (Janes *et al.* 1992, Pronin and Stofan 1990, Squyres *et al.* 1992, Stofan and Head 1990, Stofan *et al.* 1992).

Linear structural features can be divided into three classes: graben, individual normal faults, and wrinkle ridges. Graben, recognized by pairs of straight lineaments (Fig. 5), are usually associated with, and trend parallel to, the deepest portions of the chasm. The width of the graben may range from 2 to 50 km and in length from <50 to >600 km. Diffuse groups of graben (with spacings of 10–20 km) tend to occur on the flatter plains areas and near volcanic centers, while denser sets (with spacings ~2 km) are preferentially located along the chasm. Aside from concentrations near the chasm, graben are commonly located at or between coronae. Many of the graben related to coronae are sub-radial sets in corona interiors. Additionally, graben partially or completely define the annulus of at least seven coronae in the Hecate chain. Graben may also be found on the flanks of coronae

and in the plains between coronae, displaying either straight or very mildly arcuate anastomosing paths around and between the coronae.

Normal faults are found throughout Hecate and range between 50 and 400 km in length. These faults are identified primarily by radar-bright scarps. Spacings range from 15–30 km. In some locations, the vertical offset along these faults is sufficient to be seen in topography. One prominent scarp is visible near 18.5°N, 255°E (Fig. 6). This fault and several others nearby accommodate several kilometers of vertical offset along Hecate Chasma, with the north side of the fault(s) being the down-dropped side. Other distinctive scarps appear in the annuli of some coronae and in the plains bordering the chasm region.

Lineaments recognized by irregular, sinuous traces (Fig. 7) resemble wrinkle ridges found on the lunar and martian plains (Maxwell *et al.* 1975, Lucchitta 1977, Watters and Maxwell 1986). Localized sets of wrinkle ridges are found in the plains outlying Hecate Chasma, but are not necessarily prominent features. The ridges are usually only about 1–2 km across, range from tens to hundreds of kilometers in length, and are typically 10–30 km apart. Wrinkle ridges generally parallel the trend of the chasm (W–E or WSW–ENE) and predate the dominant regional fractures. It is possible that these features may be related to radial compressive stresses outboard of the topographic uplift along Hecate Chasma. At the very least, the orientation of the wrinkle ridges with respect to the trend of later structural features suggests that over time, the dominant stresses affecting the Hecate Chasma area have maintained a constant orientation.

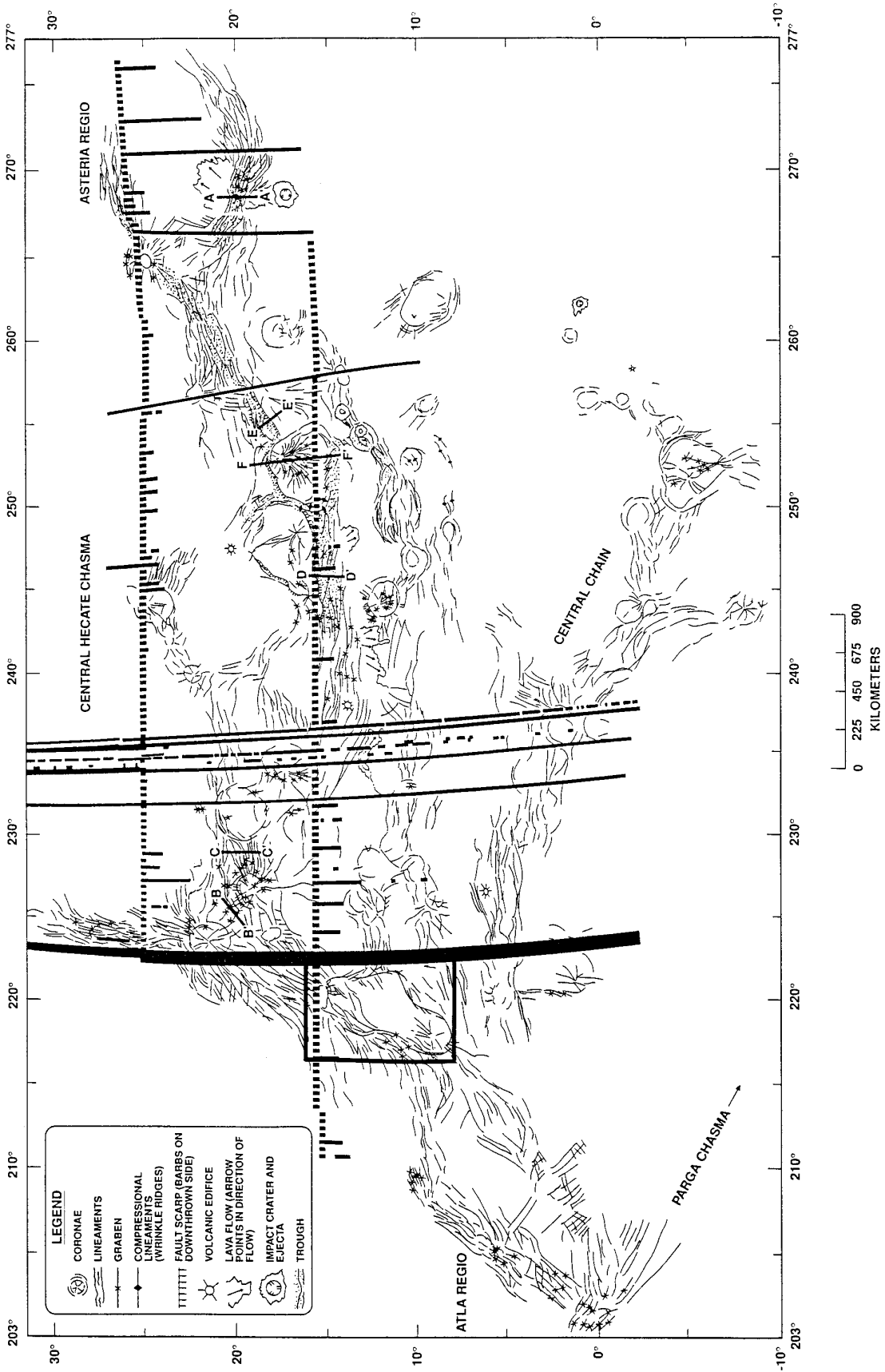
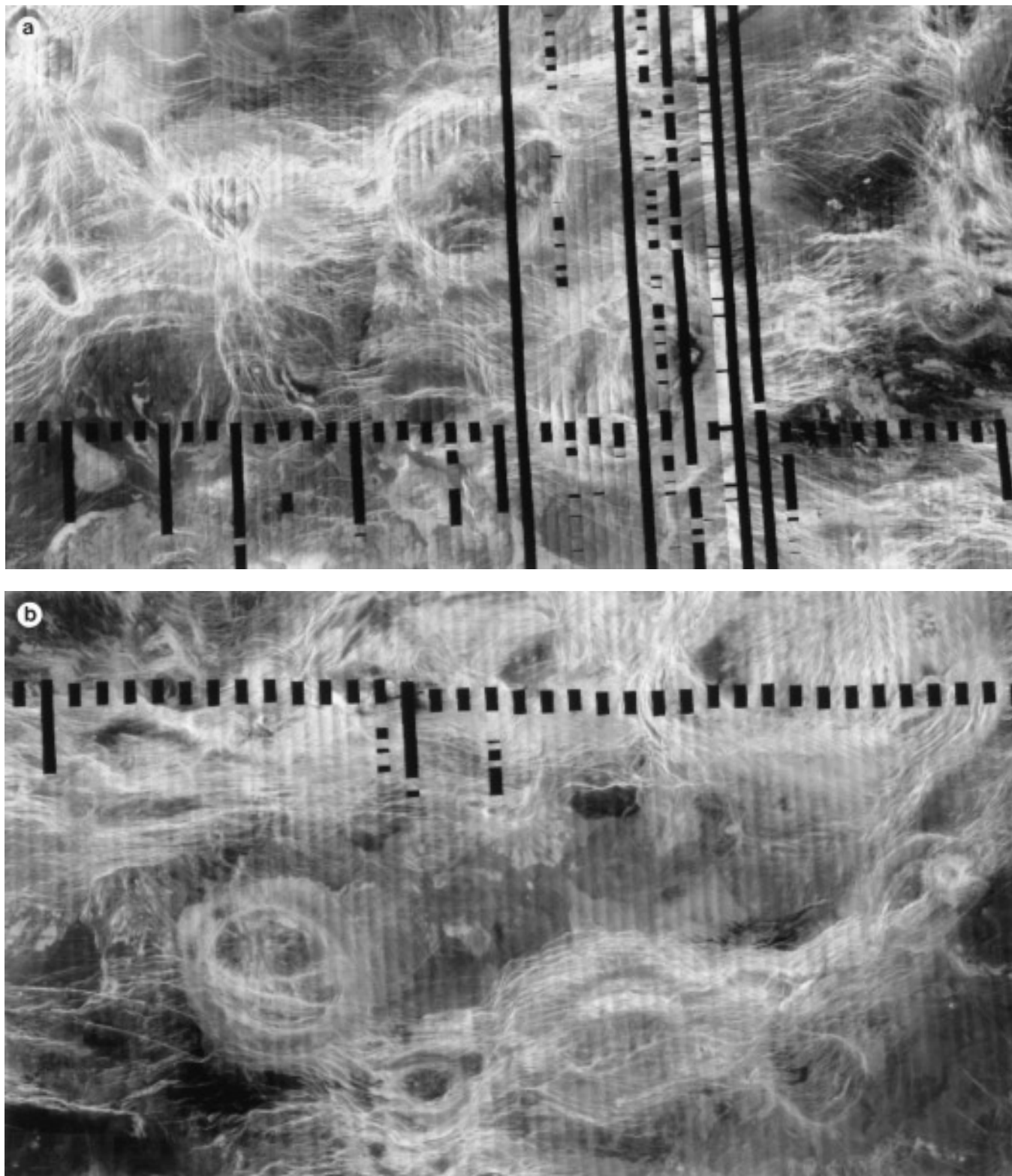


FIG. 3. Sketch map of Hecate Chasma showing dominant fracture trends, coronae, and the location of profiles discussed in this paper. The box delineates the location of Fig. 10. This map was produced from C2-MIDRPs 00N234;1, 30N232;1, and 30N284;1.



**FIG. 4.** (a) SAR image of diffusely fractured terrain. Image is centered at  $18^{\circ}\text{N}$ ,  $232^{\circ}\text{E}$  and is approximately 1680 km across. (b) SAR image of trough-dominated terrain. Image is centered at  $13^{\circ}\text{N}$ ,  $246^{\circ}\text{E}$  and is approximately 1500 km across.

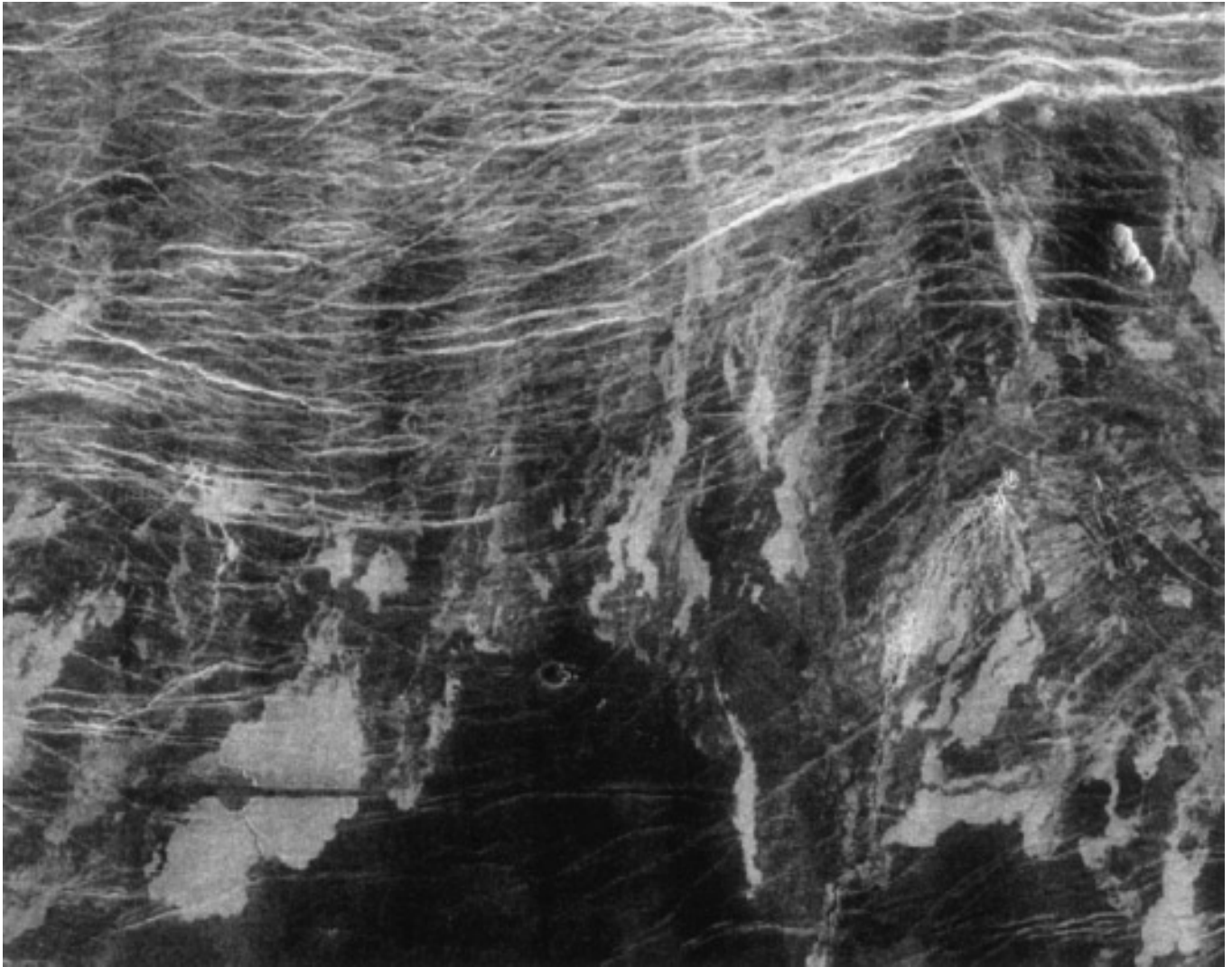


FIG. 5. Magellan SAR image of graben and associated flows in east-central Hecate Chasma. Image is centered at 12.5°N, 241°E and is approximately 150 km across.

Broad arcuate compressional ridges, another class of structural feature, are visible around the 525-km-diameter corona located at 16°N, 252°E. Compressional ridges in the annuli of coronae are uncommon, but are probably related to gravitational relaxation in the late stages of corona development (Stofan *et al.* 1991, Janes *et al.* 1992). The presence of ridges at this corona and the degraded topography support the interpretation that the corona is in the advanced stages of its evolution. Slightly less arcuate compressional fractures define four smaller coronae to the southwest of this large corona and maintain the generally east–west trend of the linear features. Because these fractures have been deflected around the annuli of the coronae, they indicate that fracturing postdated corona formation or was syntectonic.

*Volcanic features.* Throughout Hecate Chasma, several different types of lava flow units and edifices are seen: fracture-associated lava flows, small cones and cone fields, shield volcanoes, and calderas. In several areas these lava flows and edifices are embayed or cut by younger volcanic or tectonic features, while in other areas, the volcanism is the youngest event, indicating regionally contemporaneous volcanism and tectonism, or alternating periods of each.

Lava flows (Fig. 5) are commonly associated with the linear fractures, particularly graben, in Hecate Chasma. These flows are digitate and have flow directions perpendicular to and away from the local trend of deformation. These flow directions are also oriented down current topographic slopes; whether these deposits flowed onto a flat surface and were uplifted or were emplaced subsequent

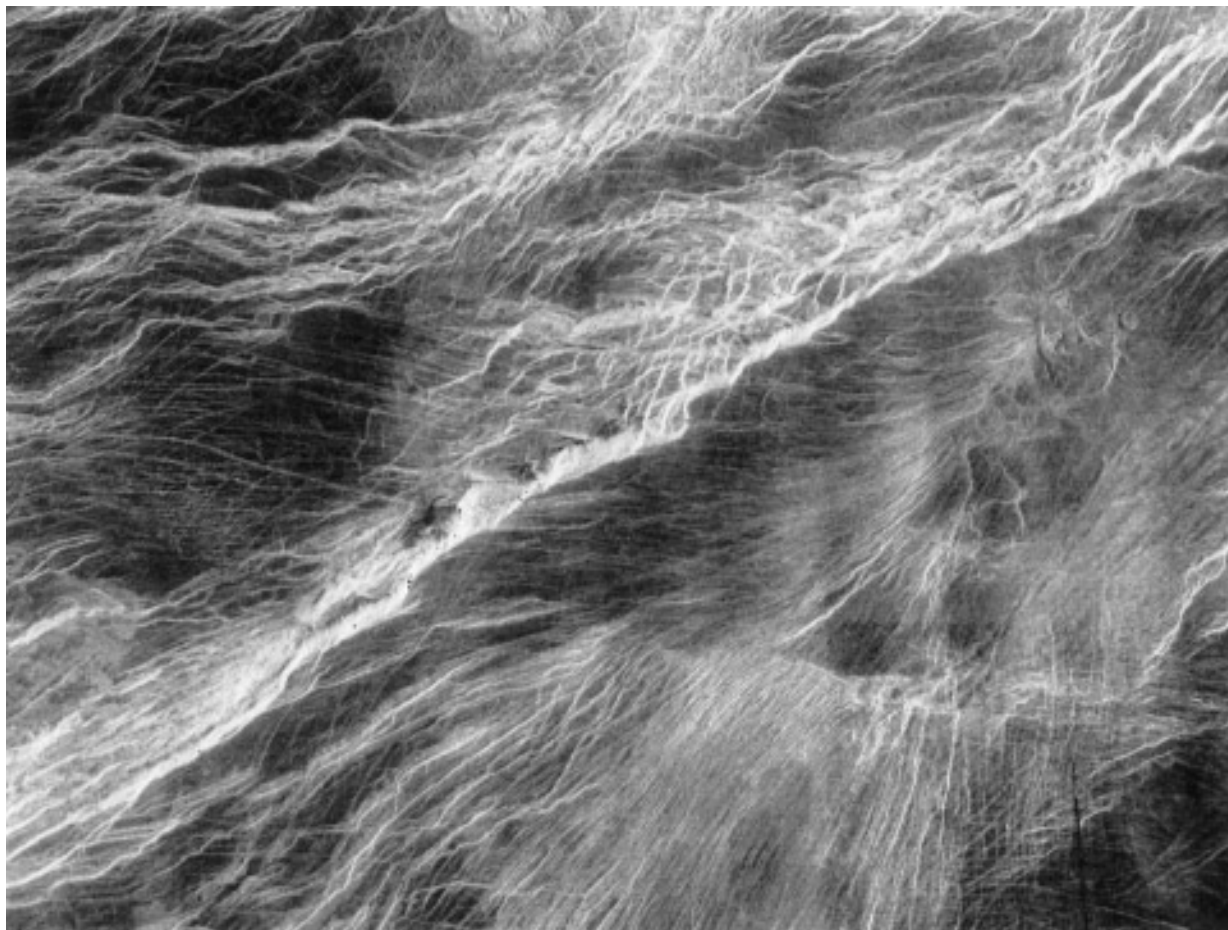


FIG. 6. SAR image of lineaments interpreted to be normal faults in east-central Hecate Chasma. Image is centered at 18.5°N, 255°E and is approximately 270 km across.

to the latest tectonism producing uplift is uncertain. Flows are usually about 150 to 200 km in length, although some have traveled up to 500 or 600 km. The radar backscatter of flows is variable within a single flow field as a result of variations in surface roughness.

Small shields and cones are prevalent in the plains between Hecate Chasma and Parga Chasma. The smallest shields and cones are about 1 km in diameter and range up to about 5 km across. Shields have small circular or elongate summit pits and are not generally characterized by radial or circumferential fracturing. Radial flows responsible for the formation of these shields are not visible at Magellan resolution. Small shields and cones commonly occur in densely populated fields hundreds to thousands of square kilometers in area. These features are typically found in the plains areas, and are not ordinarily found within areas of intense deformation. Small cones may also occur in the interiors of coronae, although this is not typical for coronae in the Hecate chain.

A few (3–5) circular calderas are also found in this re-

gion, characterized by well-defined concentric graben. Calderas are approximately 50 to 100 km in diameter. Radial flows extend for tens of kilometers around calderas. Unlike small volcanic edifices, calderas are primarily found in the deformed areas of the Hecate Chasma region, but exhibit little or no deformation themselves.

There are three major volcanic edifices in the Hecate Chasma region: Ozza Mons in Atla Regio, and two unnamed volcanoes in Asteria Regio. Ozza Mons is characterized by a large summit plateau approximately 250 km across at an elevation of 1.5 km above the surrounding plains, and extensive radial flows that extend up to 1500 km from the volcano. Several zones of linear deformation (Hecate Chasma, Parga Chasma, Ganis Chasma, and Dali Chasma) meet at Ozza Mons, forming a tectonic junction (Masursky *et al.* 1980, Schaber 1982, Senske *et al.* 1991a, 1991b). Lava flows emanating from Ozza Mons bury parts of all of these deformation zones, indicating that the volcanism at Ozza Mons has been either contemporaneous with or postdates the latest tectonism in the area.

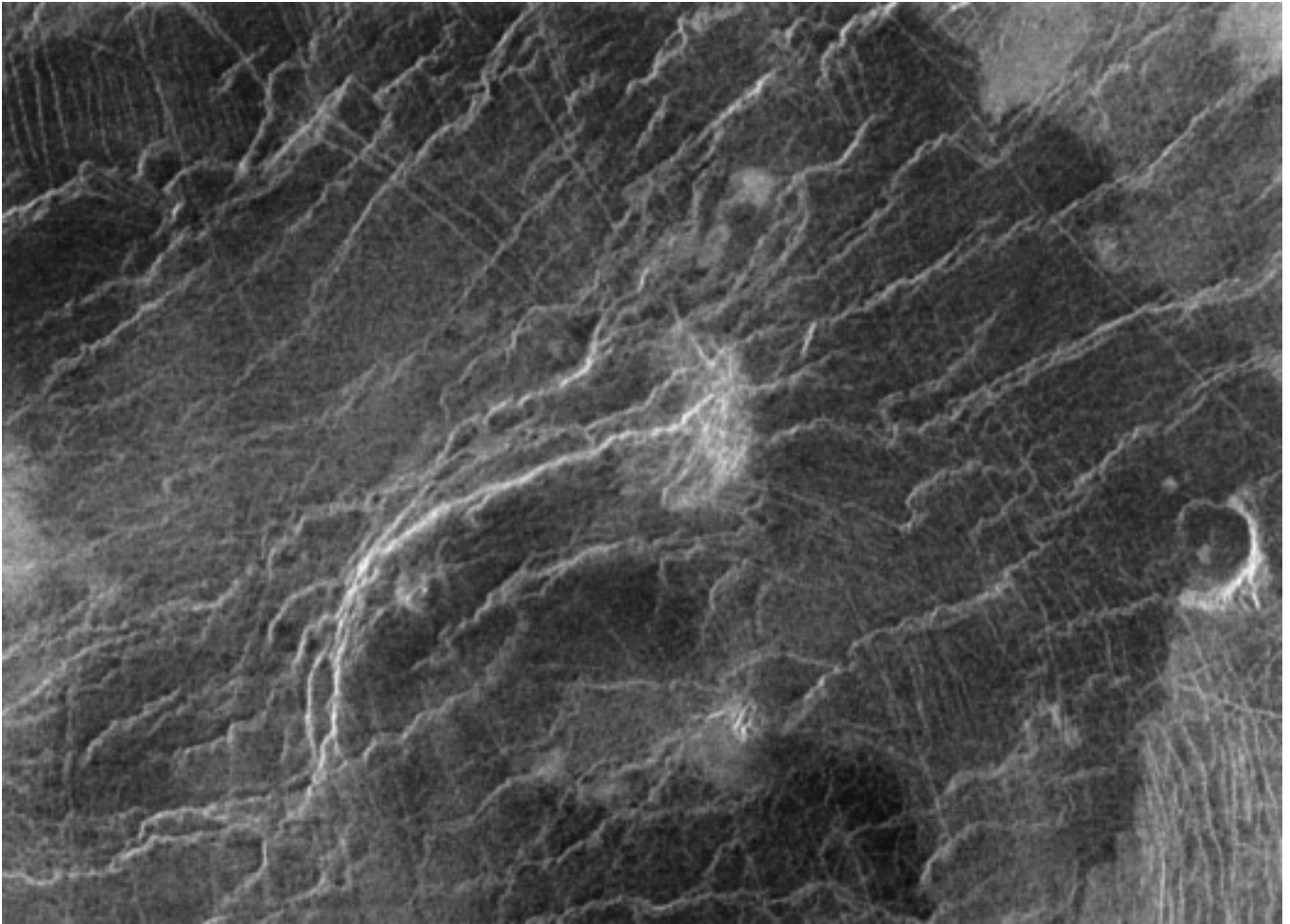


FIG. 7. SAR image of compressional lineaments in eastern Hecate Chasma. Image is centered at 21°N, 241°E and is approximately 150 km across.

The two volcanoes in Asteria Regio are smaller than Ozza Mons and differ in morphology in the case of the volcano in the east-trending arm. This volcano (Fig. 8) does not have a summit plateau, is located in a depression, and is dissected by W–E trending graben. The volcano in the NE-trending arm is located on a rise and is also heavily fractured. Normal faults are more prevalent on the upper flanks than the summit, and graben become dominant with increasing distance away from the summit (to about 200 km away).

**Coronae.** Hecate Chasma is not only notable for its distinctive topography, but also for the corona chain that lies along its length (Table I). Tectonic features associated with coronae are generally concentric; many coronae also display radial fractures. Topographic expressions include domical rises, plateaus, plateaus with interior lows, and rimmed depressions. Coronae have been suggested to have a three-stage evolution: (i) domal uplift and volcanic construction accompanied by interior deformation and radial extensional faulting, (ii) annulus and outer trough forma-

tion, continuing volcanism, and topographic degradation (plateau-form), and (iii) continued interior subsidence with rim and moat formation accompanied by volcanic flooding and embayment (Stofan and Head 1990, Stofan *et al.* 1991, Squyres *et al.* 1992) (Fig. 9).

Coronae in the Hecate chain range from 85 to over 500 km in diameter, and are defined by their heavily deformed annuli. The average spacing between coronae along Hecate is approximately 460 km from center to center, with a standard deviation of 214.4. This spacing does not appear to be distinctly related to either topographic, morphologic, or structural controls. It is possible that the emplacement of coronae and their characteristic wavelength is related to Rayleigh–Taylor instabilities at some depth; calculations for establishing approximate depth of upwelling origination are presented later in this paper.

Coronae in the Hecate chain display varying stages of evolution and do not appear to age progressively along the trend. Of 46 coronae in the chain, there are only 6 coronae which are interpreted to be in the earliest to

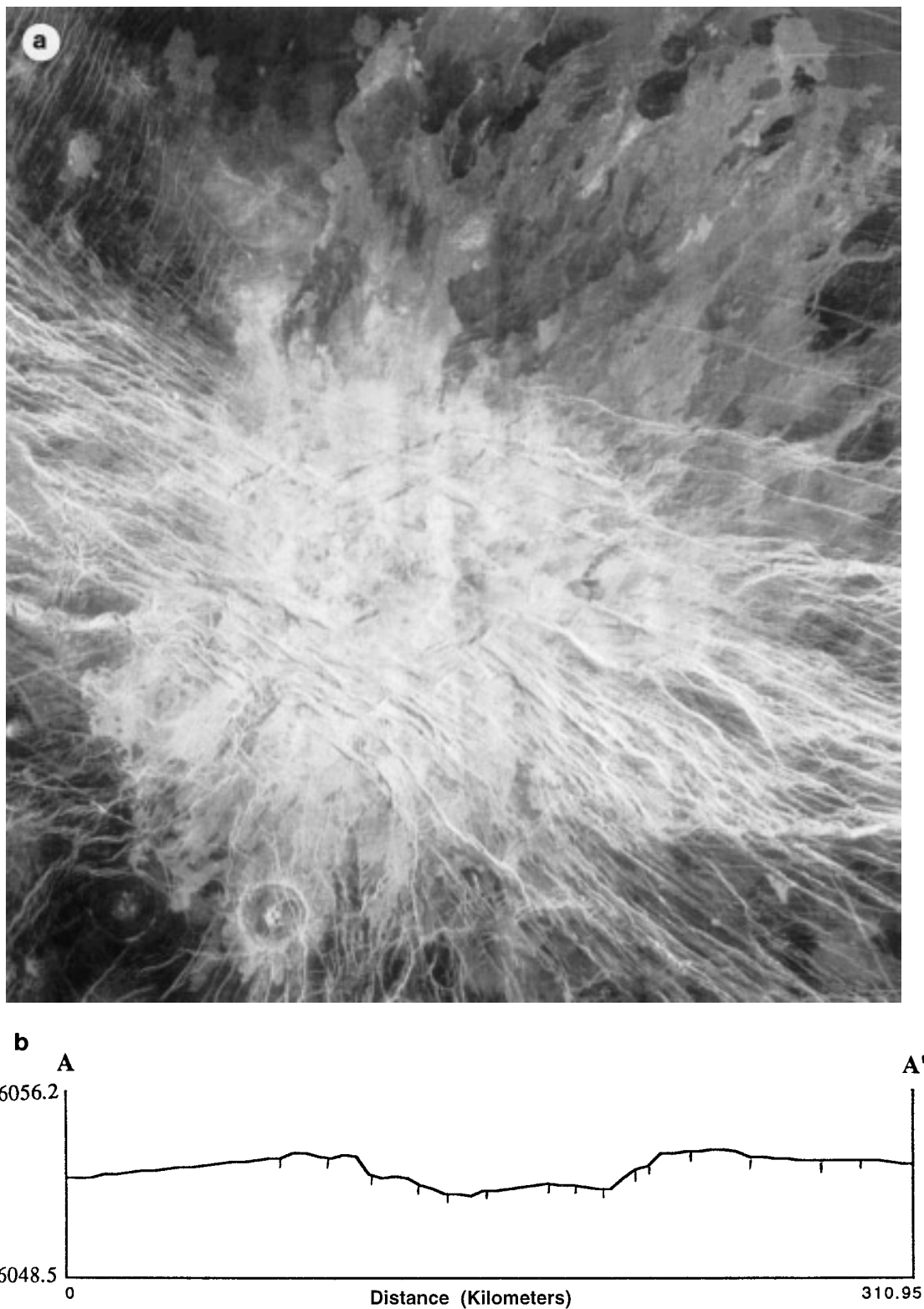


FIG. 8. (a) SAR image of unnamed volcano at  $19^{\circ}\text{N}$ ,  $269^{\circ}\text{E}$  in Asteria Regio. Image is approximately 425 km across. (b) Profile from A to A' (shown in Fig. 3) across the volcano at  $19^{\circ}\text{N}$ ,  $169^{\circ}\text{E}$ . Tick marks in this and all other profiles represent the locations of dominant fractures in the SAR image. Note vertical exaggeration in this and all subsequent profiles.

TABLE I  
Coronae in Hecate Chasma Corona Chain

Classification	Diameter (km)	Latitude	Longitude	Stage of Development	Topography	Timing
Multiple	500x225	24.0	243.5	Advanced	irregular	unknown
Asymmetric	150	22.5	256.7	Advanced	rise	pre-tectonic
Concentric	150	22.5	240.0	Early	plateau	post-tectonic
Concentric	230	22.0	226.0	Intermed./Advanced	rise	pre-tectonic
Radial/Concentric	350	22.0	224.0	Intermediate	plateau	post-tectonic
Concentric	325	20.0	231.5	Intermediate	plateau	post-tectonic
Radial/Concentric	350	19.5	227.5	Intermediate	plateau	syntectonic
Concentric	190	18.5	224.0	Intermediate	depression	pre-tectonic
Concentric	350X300	17.8	240.0	Intermed./Advanced	plateau	unknown
Volcanic	370	17.0	260.0	Advanced	rimmed plateau	unknown
Radial/Concentric	500	17.0	234.5	Intermed./Advanced	plateau	post-tectonic
Asymmetric	525	16.0	251.5	Intermediate	rimmed depression	post-tectonic
Radial	150x100	15.5	221.0	Intermediate	plateau	syntectonic
Concentric	125	14.0	258.8	Intermed./Advanced	none	unknown
Concentric	180X125	14.0	256.5	Advanced	depression	syntectonic
Concentric	125	14.0	254.5	Advanced	depression	post-tectonic
Concentric	200	13.5	253.0	Advanced	depression	post-tectonic
Multiple	300	13.0	226.5	Early/Intermed.	plateau	syntectonic
Concentric	225	12.0	238.0	Advanced	rise	syntectonic
Asymmetric	250	12.0	228.5	Advanced	depression	unknown
Concentric-DR	290	11.5	244.0	Intermediate	rimmed plateau	syntectonic
Concentric	300	11.0	248.5	Intermed./Advanced	rimmed depression	pre-tectonic
Concentric	300	10.5	251.5	Advanced	depression	pre-tectonic
Concentric-DR	200	10.0	246.0	Intermed./Advanced	depression	pre-tectonic
Concentric-DR	150	10.0	228.5	Advanced	depression	syntectonic
Concentric-DR	150	9.5	254.5	Advanced	depression	post-tectonic
Asymmetric	450x350	9.0	262.0	Early/Intermed.	rimmed plateau	unknown
Radial/Concentric	225	9.0	219.0	Intermediate	plateau	syntectonic
Concentric	150	8.0	247.5	Advanced	rimmed depression	pre-tectonic
Multiple	450x300	5.5	226.0	Intermed./Advanced	depression	syntectonic
Concentric	225	3.5	233.7	Advanced	irregular	pre-tectonic
Concentric	150x125	3.5	214.0	Advanced	depression	unknown
Asymmetric	525x300	2.5	222.0	Early/Intermed.	data gap	syntectonic
Concentric-DR	260x425	2.0	236.0	Advanced	irregular	post-tectonic
Concentric	85	2.0	218.5	Advanced	depression	unknown
Concentric	100	1.5	258.0	Advanced	irregular	unknown
Concentric-DR	160	1.0	255.0	Advanced	rise	pre-tectonic
Concentric	150	0.5	236.0	Advanced	depression	unknown
Asymmetric	125x100	0.5	241.0	Intermed./Advanced	depression	unknown
Concentric	125	0.0	240.5	Intermed./Advanced	depression	post-tectonic
Concentric	100	-1.5	255.0	Intermed./Advanced	depression	post-tectonic
Multiple	275x150	-2.0	243.0	Intermediate	irregular	syntectonic
Concentric	225	-2.0	248.0	Early/Intermed.	rimmed rise	pre-tectonic
Concentric	225	-3.0	254.0	Advanced	rise	post-tectonic
Asymmetric	500	-5.0	251.0	Intermediate	plateau	syntectonic
Radial/Concentric	350x260	-8.0	243.0	Early/Intermed.	rise	unknown

intermediate stages of development, while 10 are classified as intermediate in development, 10 are intermediate to advanced, and 20 are significantly advanced in their development (Table I) (Stofan 1993). These categories are based on topographic expression, fracture patterns, and degree of embayment. There is a good deal of subjectivity in this categorization, but we believe that it is useful and indicates that corona formation in this area has been ongoing.

Coronae commonly have substantial volcanism associated with their formation, generally in the form of radial

flows and/or interior cones and shields. Most of the coronae along Hecate Chasma have extensive volcanic deposits; only 15 completely lack or show only minor volcanism. In most cases, volcanic flows are cut by annular fractures, suggesting that the lava flows are related to early development of the corona. There does not appear to be any correlation between corona diameter and amount of volcanism or state of development.

There does appear to be a correspondence between the morphology and stage of development of many coronae and their location within one of the two morphologic ter-

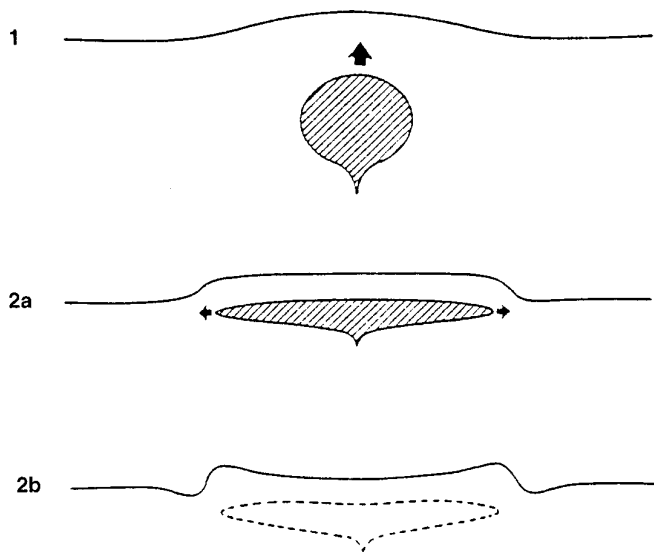


FIG. 9. Three-stage development of coronae from Squyres *et al.* (1992). Initial stage includes domal uplift, volcanism, and radial fracturing. Stage 2a begins outer trough and annulus formation and topographic degradation. Stage 2b marks the beginning of interior subsidence, flooding and embayment due to volcanism, and cross-cutting by regional tectonism.

rain types in Hecate Chasma. Coronae in diffusely fractured terrain (Fig. 4a) are typically plateaus in profile, characterized by a dominance of sub-radial fracturing, primarily large graben. The annuli of these coronae are generally poorly developed, often only encircling a portion of the corona; when discernible, the annuli are mainly defined by concentric graben or normal fault scarps. Most of these coronae are classified in the early to intermediate stages of development. Coronae in the trough-dominated regions (Fig. 4b) generally lack prominent radial fracturing, and have well-developed concentric annular fractures. Topographically, these coronae tend to have interior depressions and any raised topography is generally restricted to the annulus. The majority of these coronae appear to be in the advanced stages of development. The concentration of advanced coronae in the trough-dominated region and early to intermediate coronae in the diffusely fractured region may be evidence that the trough-dominated region is more evolved than the diffusely fractured region.

### GEOMORPHOLOGY OF HECATE CHASMA

The Hecate Chasma deformational belt can be subdivided into three geographic areas from west to east (Fig. 3): (i) Atla Regio, the western termination of Hecate Chasma and a major volcanic rise interpreted to be a hotspot (Senske *et al.* 1992, Stofan *et al.* 1995, Phillips 1994), (ii) Central Hecate Chasma, the area of dominant trough and corona

chain expression, and (iii) Asteria Regio, the eastern termination of Hecate Chasma adjacent to Beta Regio (Senske *et al.* 1992, Stofan *et al.* 1995). A chain of coronae referred to as the central chain is located between Hecate and Parga Chasmata; it is unclear whether this chain is part of Hecate, Parga, or is a separate feature. We describe here the dominant features of the geographic areas and their relations to the broader regional deformation.

### Atla Regio

Atla Regio is a regional topographic rise located at the easternmost end of Aphrodite Terra and centered near 4°N, 200°E (Fig. 1). As mentioned previously, Atla is the center of the four major convergent deformation zones of Hecate, Parga, Ganis, and Dali Chasmata. Atla Regio is interpreted to be a hotspot associated with mantle upwelling on the basis of its broad regional topography, large apparent depth of compensation (Schaber 1982, Senske 1990, Smrekar and Phillips 1991), the presence of rifts, and large volcanic edifices.

Eastern Atla Regio (Fig. 3), dominated by Ozza Mons and its flows, contains a concentration of SW–NE-trending graben which demarcate the western termination of Hecate Chasma and do not appear to be related to Ozza Mons. Almost all of the graben are either partially or completely flooded by lava flows, suggesting that most of the faulting in this area predates the most recent flow activity on the northeastern flank of Ozza Mons. Graben associated with Parga Chasma trend NW–SE and cut across the SW–NE trending faults along Hecate Chasma, indicating that deformation along Parga Chasma (at least in this region) post-dates deformation along Hecate Chasma.

Along the trend of deformation to the NE, near 12°N, 218°E, there is a distinct rift, up to 225 km wide, indicating extension perpendicular to the SSW–NNE trend of the fractures (Fig. 10). At either end of the rift, the graben forming the rift merge with the sub-radial fractures of two coronae. There are abundant lava flows emanating from this rift zone extending to the NW and SE. Although some of these flows bury older fractures, many flows have been cut by additional graben and fractures, suggesting that volcanism, rifting, and corona formation have been concurrent.

### Central Hecate Chasma

Central Hecate Chasma, containing the primary troughs and coronae in the region, includes a portion of Ulfrun Regio (between 5°N and 25°N), and can be further subdivided into western and eastern sections, both centered at about 15°N and ranging from about 210°E to 237°E, and 237°E to 265°E, respectively (Fig. 3). Both sections are characterized by a base unit of mottled plains. The domi-

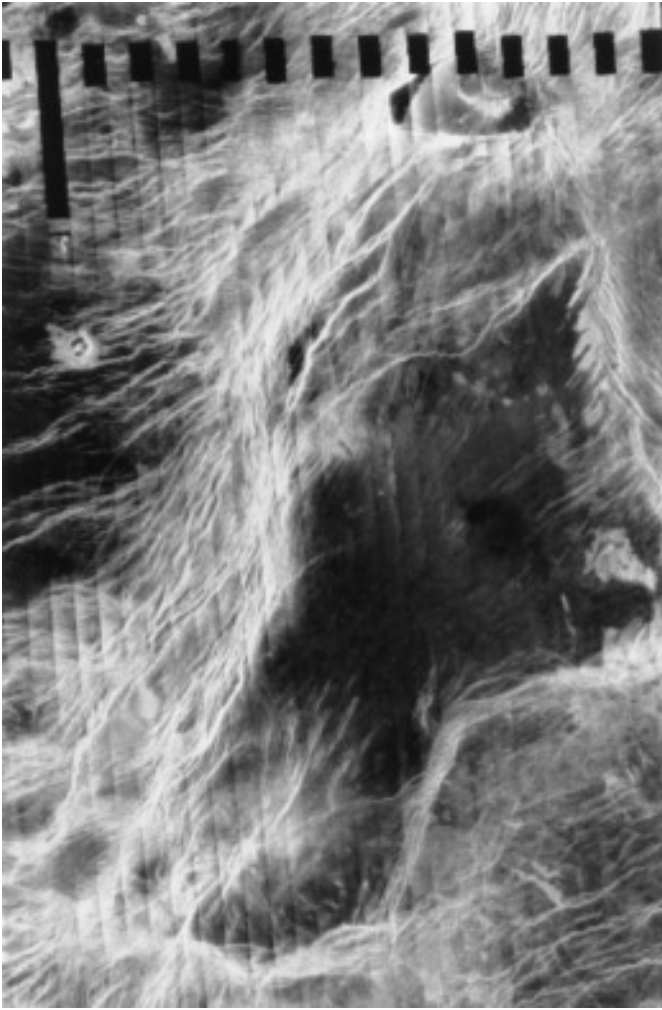


FIG. 10. SAR image of rift near Atla Regio. Image is centered at  $12^{\circ}\text{N}$ ,  $220^{\circ}\text{E}$  and is approximately 540 km across.

nant structural trend is E–W, and this trend is visible in the fractures defining the local coronae.

At least half of the coronae in the western section have extensive (usually radial) volcanic flows that are commonly fractured, indicating that tectonism accompanying corona formation has postdated volcanism. The coronae and predominant fractures in the area lie on a topographic rise at about MPR and the surrounding plains lie  $\sim 0.5$  km below MPR. In west-central Hecate, the trough is segmented and is not as distinct topographically as it is to the east. Profiles across two trough segments in west-central Hecate (Figs. 11a and 11b) display a symmetrical trough with moderately well-defined walls. The highest density of fractures is generally found in and parallel to the deepest portions of the chasm and along the walls.

The unusual, highly asymmetric main trough is particularly well-defined in the east-central section of Hecate Chasma. The 525-km-diameter corona at  $16^{\circ}\text{N}$ ,  $252^{\circ}\text{E}$  is

bounded by two segments of the WSW–ENE trending main trough (Fig. 12). To the west of this large corona, the north side of the chasm is considerably higher than the south side (Fig. 11c), and graben are chiefly concentrated on the topographically lower southern side, where they are associated with digitate flows extending to the south. To the east of the corona, the profile of the trough changes dramatically, with the higher topography on the southern side of the trough (Fig. 11d). The change in topography across the trough is great over a short distance and correlates with a series of closely spaced (10–20 km) SW–NE-trending normal faults, all with downthrown blocks on the northwest sides. Elevational changes of up to 3 km occur over as little as a few tens of kilometers of horizontal distance; this change in topography is probably accommodated incrementally by several of the larger normal faults. Several linear features cross the topographic boundary in both the eastern and western trough segments, and a few of these are offset in a manner consistent with normal faulting. The corona displays a topographic profile (Fig. 11e) consistent with advanced stages of corona development, and it is not cut by fractures from either segment of the trough. The timing relationship between this corona and the trough is unclear; the lack of trough fractures cutting the corona may be interpreted as indicating that the corona formed after the trough, or alternatively, that the corona represents a structural barrier to propagation of the trough.

To the south of the main trough, a small chain of seven coronae lies along a minor trough sub-parallel to the general trend of the main chain. This minor trough is approximately 1300 km long, lies 3.5 km below MPR at its deepest point, and does not have raised flanks. The coronae along its length are closely spaced, typically about 200 km apart, and are mostly embayed or flooded by plains volcanism, which effectively obscures any flows that may have been related to the formation of the coronae.

### *Asteria Regio*

A portion of Asteria Regio located in the area from  $23^{\circ}\text{N}$  to  $\sim 28^{\circ}\text{N}$  and between  $257^{\circ}\text{E}$  and  $\sim 273^{\circ}\text{E}$ , just west of Beta Regio, is characterized by two zones of deformation, “arms” resulting from a bifurcation of the Hecate Chasma fracture trend (Fig. 3). The SW–NE-trending arm terminates at approximately  $27^{\circ}\text{N}$ ,  $272^{\circ}\text{E}$ , to the west of Beta Regio. The W–E-trending arm branches off from Hecate Chasma at roughly  $21^{\circ}\text{N}$ ,  $260^{\circ}\text{E}$  and curves to the NE to meet Devana Chasma at the southern end of Theia Mons near  $20^{\circ}\text{N}$ ,  $276^{\circ}\text{E}$ . Neither arm has any associated coronae, but both are straddled by a single volcano.

The fractures which delineate the NE-trending arm are predominantly graben and normal faults which end fairly abruptly at the western edge of Beta Regio. The volcano

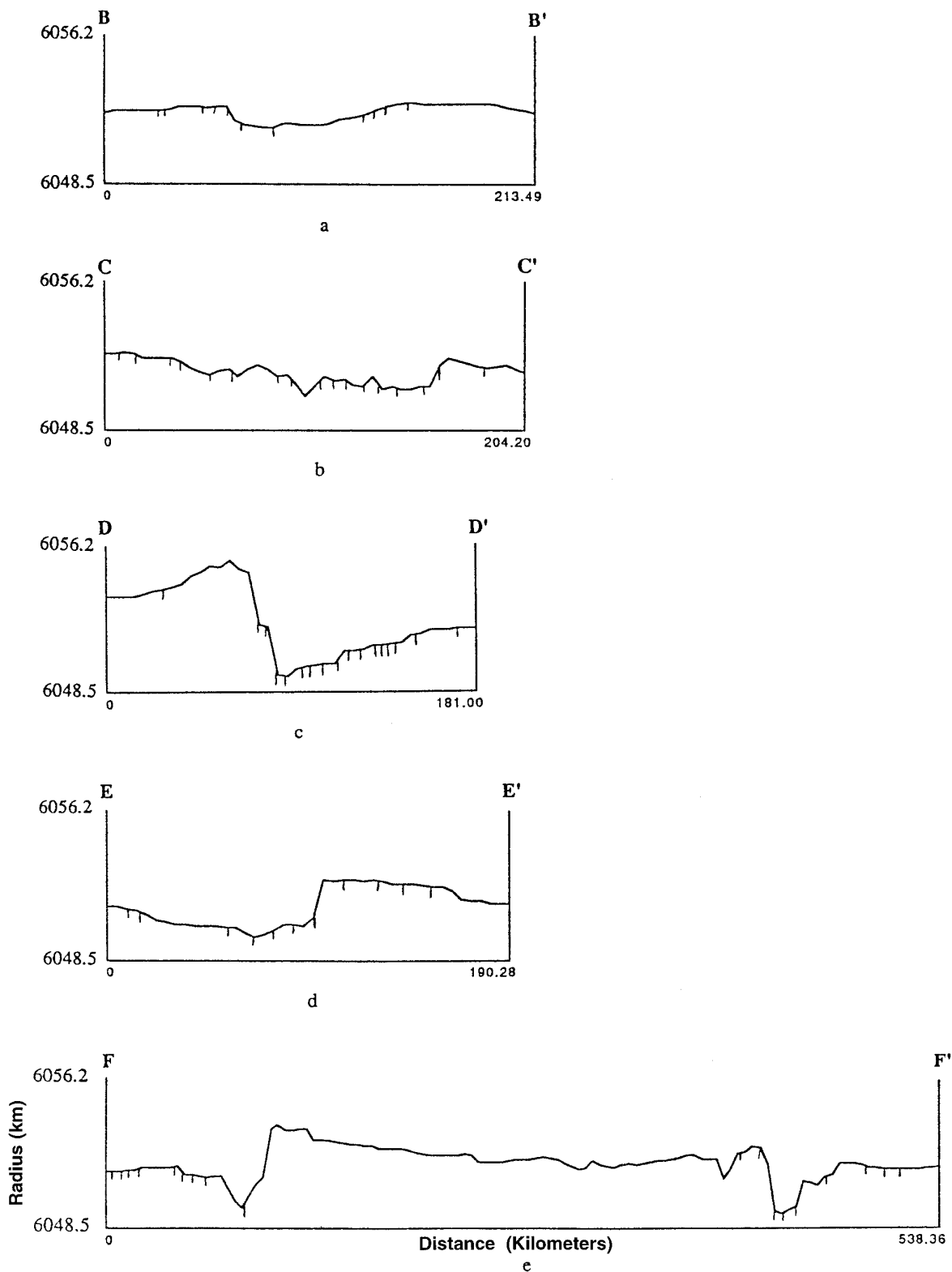


FIG. 11. (a) Profile from B to B' (shown in Fig. 3) across the trough in west-central Hecate Chasma. (b) Profile from C to C' across the trough in west-central Hecate. (c) Profile from D to D' across the western trough segment in east-central Hecate Chasma (see also Fig. 12). (d) Profile from E to E' across the northeastern trough segment in east-central Hecate. (e) Profile from F to F' across the corona at 15°N, 252°E.

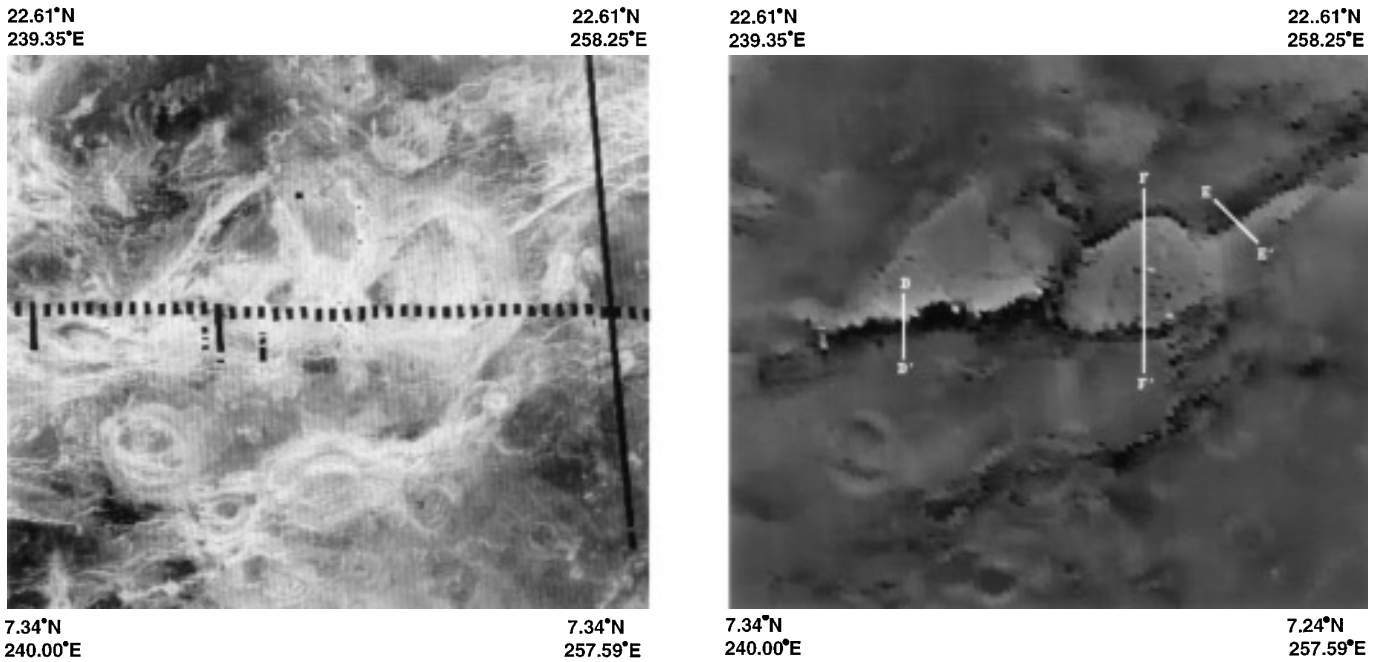


FIG. 12. (a) SAR image (C1-MIDRP 00N249;1) of east-central Hecate Chasma. (b) Topography of the region in C1-MIDRP 00N249;1 showing locations of Figs. 11c, 11d, and 11e.

in the NE-trending arm is located at 24.5°N, 264°E and has a summit diameter of 75 km. There are lava flows emanating from the summit and outlying regions, and radial fracturing is visible. Lava flows partially covering fractures near the summit imply that flows have been emplaced more recently than the fractures, which may have been formed earlier during the evolution of the volcano, potentially as the expression of subsurface dikes.

The arm trending east has a volcano along its length at 19°N, 269°E, with an approximate diameter of 100 km (Fig. 8a). This volcano is defined by an abundance of radial lava flows and high reflectivity. Graben are the predominant fractures in this arm. Fractures on the eastern side of the volcano are typically more widely spaced than those in the NE-trending arm, and curve northward to join the N–S trending fractures of Devana Chasma. The outlying plains in this area are distinctly mottled, covered by numerous lava flows probably related to smaller volcanic edifices. Volcanism locally superposes fracturing and vice versa, suggesting that the two processes have been contemporaneous.

Scarps defining normal faults are especially noticeable surrounding the two volcanoes in Asteria Regio. It is primarily these scarps which define the pattern of fracturing along this section of Hecate Chasma. Normal faults flank both volcanoes, and at the volcano at 19°N, 269°E, the normal faults become graben sets crossing the summit.

Individual scarps in this region range from 200–300 km in length. Many of the scarps anastomose, and are closely spaced, indicating that the total vertical offset is accommodated along many sub-parallel faults.

Compressional fractures occur in large groups trending SW–NE toward Beta Regio, and W–E toward Devana Chasma. The fractures in these groups are closely spaced, and anastomose throughout the region. The majority of these fractures average 300 km in length. Compressional fractures are present across the volcano in the E-trending arm, but are not found near the volcano in the NE-trending arm, where it appears that the fractures predate the volcanic activity, as stated above.

The trough follows both arms of Asteria Regio. Topography differs from that of east-central Hecate in that east of the point at which the chasm bifurcates, there is no longer a distinct asymmetry to the chasm; instead, the profile of the trough is more symmetric across the axis (Fig. 8b). The chasm walls rise up steeply to elevations as high as 6054 km on both sides, and the flanks slope away gently from the trough toward the outlying plains. The volcano along the east-trending arm is located in a depression; although it is at a slightly higher elevation than the rest of the trough, it is still lower than the flanking terrain. On the eastern side of the volcano, the trough continues to deepen to the east as it merges with the southwestern portion of Devana Chasma.

### Central Chain between Hecate and Parga Chasmata

The trend of this chain of coronae departs from the trend of western Hecate just south of the corona at 9°N, 219°E (Fig. 3). It is unclear whether this chain is branching off from Hecate, or if it is a separate feature. The trend of this chain is much straighter than along Hecate Chasma proper, and is oriented NW–SE, almost parallel to Parga Chasma. The termination of the chain is at a corona located at 5°S, 252°E, just north of Parga Chasma. Fracturing is most prevalent between 222°E and 235°E and trends predominantly W–E just as in sections of Hecate, but to the east of 235°E the fracturing is much less dense and more commonly follows the trend of the corona chain.

The fractures around and between the coronae in this chain are not typically graben, and appear to be normal faults or compressional lineaments associated with corona formation. Fracture spacings are roughly the same as for those in the main portion of Hecate, although concentrations are not as high. The coronae in this chain are slightly more widely spaced than those in Hecate, occurring an average distance of just over 600 km apart. Lava flows in the area do not appear to emanate from the fracture zone, but are associated with some coronae and volcanism in the local plains.

### MODELS FOR THE EVOLUTION OF HECATE CHASMA

The dominant attributes of Hecate Chasma which must be explained by any model include multiple wavelengths of linear deformation, troughs, lava flows, volcanoes, and the corona chain. Based on our examination of this region, we find that two models may offer explanations for the origin and events leading to the present morphology of Hecate Chasma: subduction/delamination or lithospheric extension.

#### *Subduction/Delamination*

Sandwell and Schubert (1992a, 1992b) propose a model of corona and trough formation which accounts for the present morphology of Hecate Chasma in terms of subduction and/or delamination due to thermal subsidence. This model of retrograde subduction or delamination is explained as a scenario whereby a plume head impinging on the base of the lithosphere leads to ponding of melt and hot mantle material at the surface (Fig. 13). The ponded materials cause failure of the lithosphere by loading, and the lithosphere is then predicted to sink into the mantle forming a circular subduction zone (i.e., corona) that increases its radius over time. As the interior spreads outward, a trench and outer rise develop as the result of downward bending of the lithospheric slab. Based on terrestrial analogs, Sandwell and Schubert have proposed that limited retrograde subduction may occur along arcuate

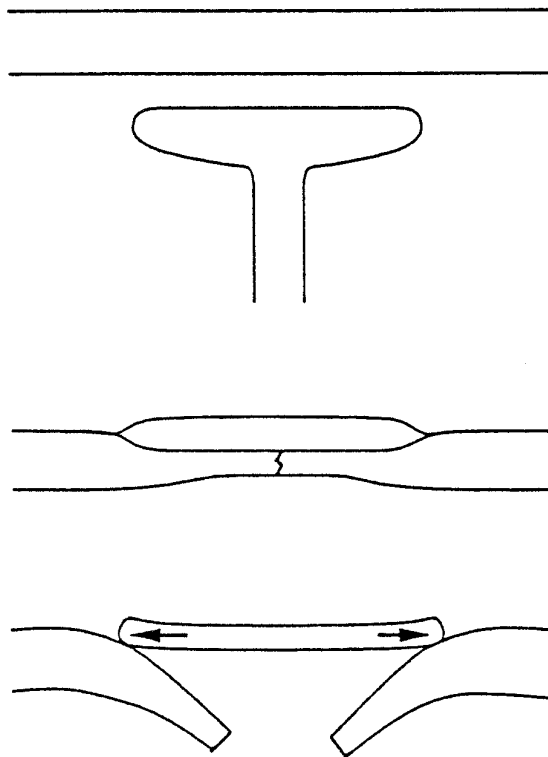


FIG. 13. Representation of the lithospheric subduction model for the formation of coronae; from Sandwell and Schubert (1992).

troughs and at the annuli of large coronae such that the corona acts like a hole in the lithosphere. The type feature for this process is suggested to be Artemis corona in Aphrodite Terra. Brown and Grimm (1995), however, found that at Artemis there is no evidence of rollback, that convergence at the annulus was uniform, i.e., not radial, and that there has only been limited underthrusting. Additionally, the Sandwell and Schubert model does not attempt to predict the types or patterns of fracturing and deformation in and around coronae that would result from retrograde subduction, and while the model can explain the broad morphology, it does not account for the detailed tectonic characteristics of coronae.

Sandwell and Schubert (1992a) state that the majority of coronae on Venus are probably too small to initiate subduction. Of the coronae along the main chasm in eastern Hecate, most are substantially smaller than the 525-km-diameter corona at 16°N, 252°E, and as such are unlikely to be large enough to initiate subduction. Profiles of these coronae also very closely match those predicted by the gravitational relaxation model for coronae (Stofan *et al.* 1991). Corona morphologies in Hecate Chasma do not match those of the coronae examined by Sandwell and Schubert; coronae in the west-central portion of Hecate have only poorly developed annular moats, when any exist at all, which would imply some other process of formation.

Additionally, most of these coronae exhibit continuous radial fractures which extend beyond the edge of a given corona rim or moat. In a subduction regime, these fractures should not extend out continuously beyond the trench, unless they formed prior to subduction, in which case they should display considerable offset or difference in orientation on either side of the trench (Hansen and Phillips 1993). Coronae along Hecate Chasma are highly circular and do not display evidence of expansion in their interiors, which is expected in the retrograde subduction model as a result of the growth of the corona as the outlying lithosphere rolls back. While upwellings are postulated by Sandwell and Schubert to result in subduction, a concentrated zone of upwellings along Hecate Chasma suggests that the region is one of higher heat flow and warmer lithosphere than average, conditions which should inhibit subduction at coronae.

In addition to coronae, Schubert and Sandwell (1995) also suggest that the trough segment west of the large corona at 16°N, 252°E is a site of potential subduction. We emphasize here that, in general, caution is advised in applying plate tectonic processes to Venus when it is possible to describe other processes that might generate similar features. However, if the subduction process is invoked to describe this area, we feel that the geological features observed in the area must then meet the expectations of such a zone. Our argument against classifying this region as a subduction zone is thus based, in part, on features expected at a plate tectonic boundary. McKenzie *et al.* (1992) point out that if large amplitude features are in fact subduction-related trenches, they must terminate on transform faults in the same way that they do on Earth. If the main asymmetric trough through eastern Hecate Chasma is a subduction boundary, the change in the topographic asymmetry from north to south on either side of the corona at 16°N, 252°E (Fig. 12) is difficult to explain unless there is a transform that separates northward convergence in the west from southeastward convergence in the east. However, there is no evidence for a transform in or on either side of the corona between the trough segments. Similarly, because the trench does not extend infinitely away from the corona, it must have ends along transform boundaries; observations of this chasm do not provide any evidence of major high-angle faults at the ends of the trough or anywhere in between.

The majority of features along Hecate Chasma do not appear to fit the subduction/delamination model. Along the trend of the chasm and running parallel to it on both sides, there are numerous sets of paired lineaments which are interpreted to be graben. Extensional features may locally cross the trend of the trough without exhibiting deflection or displacement, suggesting that subduction is not occurring. Nearby, digitate lava flows appear to originate from the graben and flow to the north and south of

the main trough. This extensional morphology and linked volcanism on both sides of the trough is difficult to reconcile with subduction activity. Volcanism expected at a subduction zone is typically located on the overriding plate forward of the subducting slab, not on both sides of the trench. Extension might be observed on the subducting plate as a result of tension due to flexure of the lithosphere as it descends; however, volcanism is not expected to accompany this extension, nor is extension likely to dominate on the leading edge of the overriding plate (in the absence of an accretionary wedge), characteristics found in this region of Venus.

How the subduction/delamination process fits into a global tectonic regime is a complex issue that has not been fully explored. If the process is only occurring at certain large coronae on Venus, the implication is that there is more than one type of corona (i.e., subducting and non-subducting). If this is the case, the types do not appear to be distinguishable, nor have any transitional features been identified. Also, many coronae on Venus do not have a trench as part of their annulus, implying yet another type of process. As mentioned earlier, Sandwell and Schubert state that in the process of delamination, the corona grows as the lithosphere rolls back, however, it seems that the continued upwelling would tend to oppose the downward motion of the slabs (assuming they are negatively buoyant to begin with), or even cause partial melting of the slabs. In addition, the interior surfaces of many coronae do not appear to have been breached by upwelling material and do not display the massive lava flow morphology implied by Sandwell and Schubert's model. Sandwell and Schubert (1992a, 1992b) recognize that the downwarping around coronae does not require subduction, that it may in fact be the product of overthrusting of the exterior lithosphere by the corona, or the result of gravitational relaxation as proposed by Stofan *et al.* (1991) and Janes *et al.* (1992). Finally, McKenzie *et al.* (1992) consider that if all of the large troughs and/or chasmata on Venus represent subduction zones, there must be an assemblage of equally prevalent features related to processes generating new surface material, and there is currently no evidence for such a system.

#### *Lithospheric Extension with Limited Rifting*

The second model proposes that Hecate Chasma has been formed by regional extension accompanied by localized rifting and corona formation. Rift zones are characterized by volcanic flow piles, concentrated fracturing, and vertical displacement due to normal faulting. Fissures and faults that run parallel to the axis of a rift are the result of tension due to extension. In profile, rift segments generally look like troughs with steep walls and may or may not appear symmetrical depending on the nature of the faulting

and the response of the lithosphere to stress. The presence of a major trough with parallel normal faulting and associated outflows at Hecate Chasma is consistent with other venusian (Baer *et al.* 1994, Senske *et al.* 1991a, 1991b, 1992) and terrestrial (e.g., Vening Meinesz 1950) rift morphologies. The main portion of the chasm has an asymmetric profile marked by extreme vertical variations in topography that can be accounted for by uneven normal faulting (Senske *et al.* 1992). Therefore, we interpret the geologic evidence at Hecate Chasma to support a lithospheric extension model.

*Multi-wavelength deformation.* The long wavelength of deformation along Hecate Chasma is defined by the localized chain of coronae, the chasm, and the areally restricted fracture zone. The typical width of the fracture zone is approximately 200–400 km. Individual faults and graben sets define the short wavelength of deformation and their spacing is generally 2–30 km. The model of Zuber *et al.* (1986) and Zuber (1987) may be able to explain the multiple wavelengths of deformation observed along Hecate Chasma.

The subsurface layering model of Zuber (1987) suggests that the venusian lithosphere is comprised of a strong upper layer underlain by a weak lower layer superposed on a strong upper mantle. Changes in strength, heat flow, and thickness of the crust with time are not accounted for in this model. This layering produces two wavelengths of deformation; a long wavelength (hundreds of km) related to the response of the lithosphere to extension, and a short wavelength (tens of km) resulting from deformation of the crust. Two-dimensional topography predicted by this model (given a lower limit for thermal gradient of 10 K km<sup>-1</sup>) places an upper bound on crustal thickness at 30 km for a region with two wavelengths of deformation. For a thicker crust, there would not be a region of upper mantle strength, and only one, short wavelength of deformation would be seen.

Detailed knowledge of the interior structure of Venus is needed to fully understand the application of this model to local tectonics. Although nonunique and probably not applicable globally, the model is consistent with the suggestion that the tectonic features we have seen in Hecate Chasma can be explained by extensional tectonism.

*Sequence of events and morphologic terrains.* In order to assess the relationship between corona formation, tectonism, and morphologic region, coronae along Hecate Chasma were classified as pre-tectonic, syntectonic, or post-tectonic on the basis of superposition relationships between the coronae and regional fractures and volcanism. If regional fractures terminate against the fractures of a corona (e.g., a “T-junction”), the corona-related fractures are presumed to be preexisting fractures which provide a structural barrier to the propagation of the

regional fractures. Also, if regional fractures are deflected around a corona, the corona is presumed to have formed first (pre-tectonic). If local fractures superpose corona flows, and corona fractures or flows also superpose local fractures, the corona is presumed to have formed syntectonically. If regional fractures are clearly superposed by corona fractures or flows, then the corona is considered post-tectonic. The syntectonic classification is only representative of the latest relationship evident, as these coronae may have formed prior to major tectonic fracturing, but show evidence of subsequent activity concurrent with tectonism.

The results of the classification are shown in Table II. The first trend to note is that of the 46 coronae, there is a roughly even division among the pre-, syn-, and post-tectonic classes, suggesting that coronae have been forming throughout the evolution of this area, that tectonism does not unilaterally predate or postdate corona formation, and that tectonism in the region is not very uniform or well-organized. Coronae are also classified as to the geographic/morphologic region (see earlier discussion) of their occurrence, being divided into concentrated and diffuse fracturing regions, and central chain coronae. Each of the three groups contains roughly one-third of all coronae, indicating that there is no preferential concentration of coronae in any geographic subregion of Hecate Chasma. In the region of diffuse fracturing, 36% of coronae are classified as syntectonic, 14% are classified as pre-tectonic, and 29% as post-tectonic. In the region of concentrated fracturing, 14% are syntectonic, 36% are classified as pre-tectonic, and 29% are considered post-tectonic. Due to the small number of coronae in each area, and the fairly even distribution among the pre-, syn-, and post-tectonic classes, we believe these percentages to be inconclusive regarding a dominant regional timing relationship between corona formation and local fracturing.

The heterogeneity of relationships between tectonism and corona formation indicates that even locally, tectonism and corona formation have been concurrent. Baer *et al.* (1994) examined the relationship between coronae and extensional belts in northern Lada Terra and found similar evidence that some of the coronae may have influenced the location of surface expressions of regional extensional stresses, and that conversely, the extensional stresses may have influenced the locations of other coronae. These relationships indicate that the extensional and corona-forming processes in extensional environments are closely connected to one process, and support the idea that neither corona formation nor extension can be said to drive the other.

Although within each morphologic setting there is no definitive temporal relationship between tectonism and corona formation, it is possible that the two settings are representative of two stages in the evolution of an exten-

TABLE II  
Classification of Coronae with Respect to Tectonism

Class	All coronae (46 = 100%)		Concentrated and diffuse only (28 = 61%)		Concentrated only (14 = 30.4%)		Diffuse only (14 = 30.4%)	
	# Coronae (of 46)	Percentage	# Coronae (of 28)	Percentage	# Coronae (of 14)	Percentage	# Coronae (of 14)	Percentage
Pretectonic	11	24%	7	25%	5	36%	2	24%
Syntectonic	11	24%	7	25%	2	14%	5	36%
Posttectonic	12	25%	8	29%	4	29%	4	29%
Unknown	13	28%	6	21%	3	21%	3	21%

sional zone, with the broadly extending region representing the initial stages, characterized by dispersed, regionally accommodated extension, and the region of concentrated extension as a more evolved zone distinguishable by more localized tectonism and volcanism. Much like Hansen and Phillips (1993) found in eastern Aphrodite Terra, it appears that the morphologies of these portions of Hecate Chasma are the result of a combination of regional extension coeval with corona formation and shallow (lithospheric) magma bodies whose upwellings have been aided by the regional stress field (Stofan *et al.* 1993, Hamilton and Stofan 1994).

Compressional features found in locations other than corona annuli are not specifically accounted for in our model. As most of these compressional structures predate extensional structures, it is possible that they are related to an earlier tectonic regime. Structural orientations are such that the principle compressive stress of the first tectonic regime was oriented parallel to the principle tensional stress of the current regime, suggesting that there may be a significant structural weakness in the lithosphere along an E–W, WSW–ENE trend in the region between Atla and Beta Regiones.

*Rayleigh–Taylor instabilities and corona formation.* Models of corona formation attribute the distinctive surface manifestation of coronae to upwelling diapirs that originate in the mantle and impinge on the base of the lithosphere (Stofan *et al.* 1990, Stofan *et al.* 1992, Squyres *et al.* 1992, Janes *et al.* 1992). Stofan *et al.* (1992) discuss the general characteristics of coronae and their formation by mantle plumes, but do not explicitly address the issue of the specific depths at which these plumes originate. Comparing the generally small sizes and short life spans of coronae to large, known hotspots such as Beta, Eistla, and Atla Regiones (e.g., Bindschadler *et al.* 1992, Grimm and Phillips 1992), it is unlikely that coronae originate as deeply as the core–mantle boundary. Other workers have proposed that coronae may be the result of upwelling diapirs within the upper mantle (Herrick and Phillips 1992, Tackley *et al.* 1992, Hansen and Phillips 1993) or specifically as Rayleigh–Taylor instabilities (Tackley and Stevenson

1991, Tackley *et al.* 1992). Herrick and Phillips (1992) found an anticorrelation between the locations of coronae and high amplitude mantle upwellings and downwellings, indicating that any link between coronae and mantle convection is complex. They propose that coronae may be passive features related to lithospheric extension and the magmatism that accompanies thinning. Lithospheric thinning could produce zones of partial melting as a result of adiabatic decompression (Tackley and Stevenson 1991, Tackley *et al.* 1992), with large magma bodies forming coronae at the surface.

Globally, the average spacing between coronae is approximately 670 km (Stofan *et al.* 1992), while in the Hecate Chasma region, the average spacing between coronae is about 460 km. The Hecate Chasma spacing is closer than the global average, and the concentration of these coronae along a fairly linear deformational trend is significant. Determination of the size of the diapirs and the depth(s) from which they originate may provide information about their relationship with the tectonics of Hecate Chasma.

It is possible that the characteristic wavelengths associated with groups of coronae may be explained by Rayleigh–Taylor gravitational instabilities in the lower crust or mantle. Instability due to a heavy, dense layer underlain by a lighter, less dense layer results in diapiric upwelling of the lower density layer with a characteristic spacing between diapirs. Models of this behavior may or may not assume an isoviscous plume and overburden layer (e.g., Koch 1994, Whitehead *et al.* 1984, Bonatti 1985, Crane 1985).

Although few parameters are known for Venus' interior structure and values of viscosity, density, thermal gradient, etc., it may be assumed that the uppermost part of the planet is nonisoviscous. However, we have used two existing models, isoviscous and nonisoviscous (Turcotte and Schubert 1982, Koch 1994, Bonatti 1985, Schouten *et al.* 1985, Crane *et al.* 1985), to describe the depth of plume origination based on the spacing of coronae along Hecate Chasma. Although there are significant differences between the two models, we find that they are generally in agreement in terms of the values determined for depth to the instability and diapir size.

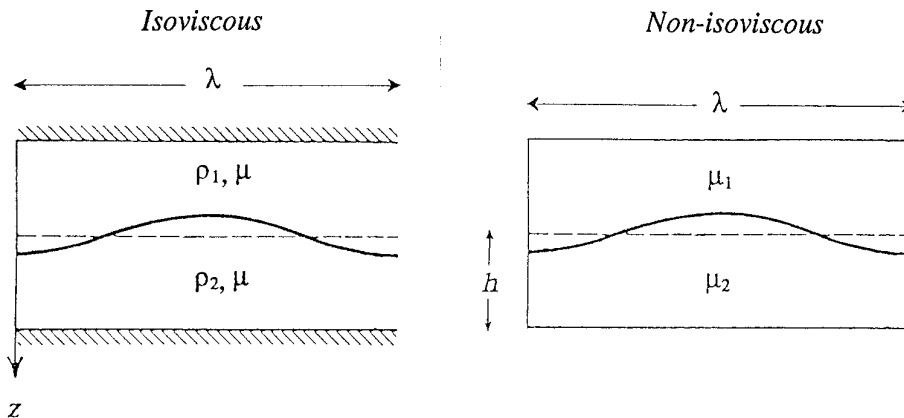


FIG. 14. Schematic representations of the isoviscous (left) and nonisoviscous (right) models of Rayleigh–Taylor gravitational instabilities. Modified after Turcotte and Schubert (1992).

Deficiencies in the amount of data available must be taken into account when applying Rayleigh–Taylor instability theory to the formation of a corona chain on Venus. Corona spacing, although reasonably consistent, is by no means as regular as the volcanic spacings examined along mid-ocean ridges on Earth, and may be the result of additional influences on the path of upwelling diapirs. In addition, corona chains are located along or near tectonic features which are less continuous and less clearly defined than mid-ocean ridges on Earth. In light of these relationships, and the lack of knowledge of the interior structure of Venus, we strongly advise caution in taking calculated values presented here as absolutes.

The growth time of the disturbance between two layers depends on the wavelength of the interface distortion of the layers; the disturbance with the shortest time constant grows and dominates the instability. The wavelength that gives the smallest values for the time constant is related to the depth of the layer for isoviscous upper and lower layers (Turcotte and Schubert 1982, Eq. 6–161),

$$\lambda = 2.568 \cdot z, \quad (1)$$

where  $\lambda$  is the characteristic wavelength of the upwellings and  $z$  is the depth to the lower instability (Fig. 14). When the characteristic spacing along the main portion of Hecate Chasma ( $457 \pm 28$  km) is used in Eq. (1) to solve for the depth to the instability,  $z$  is found to be approximately  $178 \pm 11$  km (Table III).

Variable-viscosity models determine wavelength as related to the ratio of the thicknesses of the layers and the ratio of their viscosities. Several workers (Whitehead *et al.* 1984, Crane 1985, Bonatti 1985, Schouten *et al.* 1985) have modeled the spacing of upwellings and volcanism at terrestrial mid-ocean ridges as characteristic wavelengths produced by upwellings due to Rayleigh–Taylor instabilities.

Crane (1985) and Bonatti (1985) provide the equation relating wavelength to the viscosity ratio between the layers and the thickness of the unstable layer,

$$\lambda = \frac{2\pi h}{2.15} \left( \frac{\mu_1}{\mu_2} \right)^{1/3}, \quad (2)$$

where  $\lambda$  is the wavelength of the features in kilometers,  $h$  is the thickness of the lower layer, and  $(\mu_1/\mu_2)$  is the ratio of the layers' viscosities (Fig. 14). The value most commonly cited for  $(\mu_1/\mu_2)$  is  $10^3$  (Rabinowicz *et al.* 1984, Bonatti 1985, Crane 1985). This ratio is based on terrestrial models that predict a steep viscosity gradient across the base of the partial melt zone (the most likely source for the instability), where the lower layer of initial melt is of lower viscosity than the overlying layer.  $\mu_1$  is assumed to be on the order of  $10^{20}$  P, and  $\mu_2$  estimated as lower by 2–4 orders of magnitude (Lewis 1981, Rabinowicz *et al.* 1984, Bonatti 1985).  $\mu_2$  is variable with the values chosen for the degree of partial melting of the buoyant layer and

TABLE III  
Comparison of Rayleigh–Taylor Instability Models

Variable	Model		
	Isoviscous	Isoviscous	Nonisoviscous
Average corona diameter (km)	240	240	240
Depth to instability (km)	180	180	157
Thickness of instable layer (km)	18 <sup>a</sup>	18 <sup>a</sup>	15.7
Factor of plume spreading	3	1.5	N/A
Diapir size (km)	80	160	88

<sup>a</sup> Thickness of instable layer from nonisoviscous model.

the temperature and pressure contrasts of the unstable and overlying layers. The general trend of the function is for  $h$  to increase with decreasing viscosity contrast. The thickness ( $h$ ) of the lower unstable layer is assumed to be less than at least  $\frac{1}{10}$  the depth to that layer (Biot and Odé 1965, Crane 1985). From Eq. (2), for the average 457 km spacing along Hecate Chasma, a calculated layer thickness of 15.6 km would then correlate to a depth of 156 km (Table III).

Both isoviscous and nonisoviscous models also provide methods for calculating the diameter of plumes resulting in coronae. Koch (1994) has modeled the effect of an isoviscous plume encountering a free fluid surface. The plume is a roughly spherical spreading drop with a trailing tail that is not attached to a continuous source. Koch does not use the model in order to predict diapir diameter, but based on the author's estimations of plume flattening, we estimate plume diameter based on the diameter of the surface feature. Once the surface has attained a plateau-like topographic profile, Koch assumes that the flattened plume head diameter is roughly the same as that of the surface feature, and that plume diameter may increase by as much as a factor of 3 once it flattens. The average diameter of the coronae along Hecate Chasma is 240 km. If we assume that all coronae are at or beyond the stage of forming topographic plateaus and the maximum amount of plume flattening has occurred ( $3\times$ ), the average diapir diameter can be estimated to be approximately 80 km. If, however, we assume that the majority of coronae have not completely flattened and their plumes have only spread to  $1.5\times$  their original diameter, then the average diapir diameter is closer to 160 km. Janes *et al.* (1992) modeled diapiric uplift for five coronae (-like) features and found that diapirs for features of various sizes were all estimated to be less than 200 km in diameter (originating below an elastic lithosphere between  $<10$  and 30 km thick); thus the plume diameters estimated here are in agreement with the range of values established by their model.

Crane (1985) modeled diapir diameter at mid-ocean ridges as a function of the thickness of the buoyant layer and the viscosity ratio:

$$d = h \left( \frac{\mu_1}{\mu_2} \right)^{1/4}. \quad (3)$$

Diapir size is thus expected to increase with increasing thickness of the unstable layer. Again using  $(\mu_1/\mu_2) = 10^3$ , and  $h = 15.6$  km, plume diameter is calculated as approximately 88 km, a value consistent with the range of values determined by Janes *et al.* (1992) and our calculations based on isoviscous layers.

Table III shows calculated values of depth to the instability, thickness of the instable layer, and diapir size for both the isoviscous and the nonisoviscous models as applied to

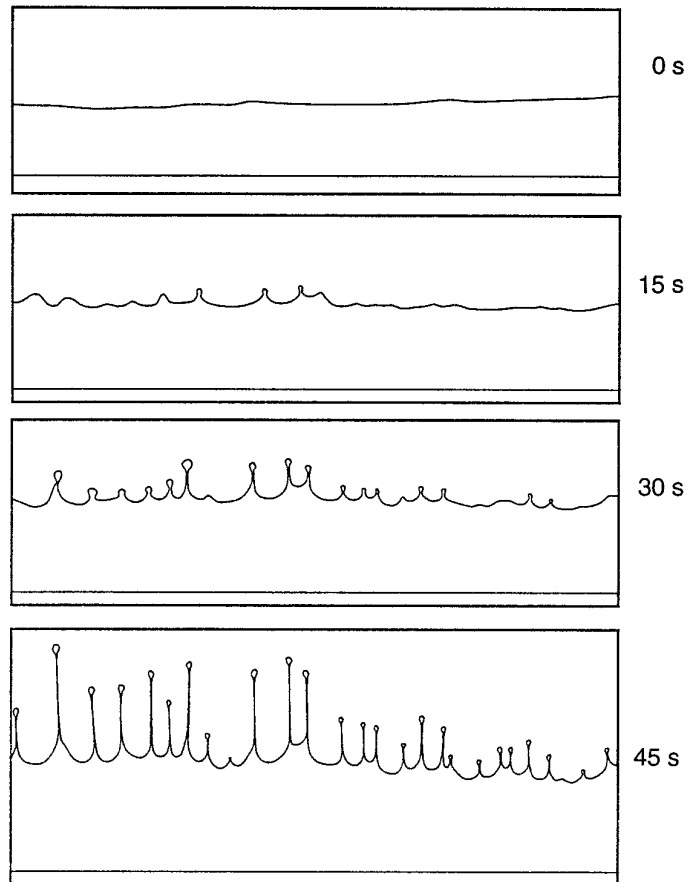


FIG. 15. Water/glycerine diapirs in glycerine bath. After Whitehead *et al.* (1984).

coronae in Hecate Chasma. For the isoviscous situation, we have also calculated a second value of diapir size under the assumption that the source plumes of coronae in the intermediate stages of development may have only spread to  $1.5\times$  their original diameter. The thickness of the instable layer calculated for the isoviscous model is based on the assumption (from the nonisoviscous model) that the thickness of that layer is equal to or less than  $\frac{1}{10}$  the depth to that layer.

We acknowledge that some degree of simultaneity in upwelling is implied by the Rayleigh–Taylor model. We interpret the coronae in this region to have evolved simultaneously in that virtually all of the coronae presumably formed since the last catastrophic resurfacing event ( $\sim 300$ – $500$  Ma) and are apparently commonly related to the extension along Hecate Chasma. However, these relations do not preclude local variations in age or stage of evolution. Figure 15 shows the gravitational instability of a horizontal line of water/glycerine mixture in a bath of pure glycerine. The rates of ascent of the instabilities/diapirs are clearly not all equal, even though they all origi-

nated at the same depth at the same time. We believe that this behavior accounts for the variation in corona development along Hecate Chasma.

## CONCLUSIONS

There are a wide variety of tectonic and volcanic features present in and along Hecate Chasma, including a distinctive chain of coronae presumed to be the surface expressions of upwelling diapirs. We draw three main conclusions about the deformation in Hecate Chasma; (i) fractures defining the zone of deformation are dominantly extensional, (ii) there appear to be two morphologically distinct regions along Hecate Chasma, and (iii) formation and spacing of coronae may be controlled by gravitational instabilities at shallow depths in the mantle.

*Extensional deformation.* The predominance of features related to extension and upwelling implies that the tectonic features of this region are the result of lithospheric extension. The presence of a major trough with parallel normal faulting and associated outflows at Hecate Chasma is consistent with other venusian (Baer *et al.* 1994, Senske *et al.* 1991a, 1991b, 1992) and terrestrial (e.g., Vening Meinesz 1950) rift morphologies. The main portion of the chasm has an asymmetric profile marked by extreme vertical variations in topography that can be accounted for by uneven normal faulting (Senske *et al.* 1992), further suggesting lithospheric extension.

*Morphologic terrains.* The two morphologic settings discussed earlier may be representative of two stages in the evolution of an extensional zone, with broadly extending regions representing the initiation of rift tectonism and highly concentrated regions of fracturing as evolved zones of rifting distinguishable by more localized tectonism and volcanism. In both morphologic areas, there is evidence that fracturing and/or extension predated the formation of coronae and influenced their location of emplacement; conversely, evidence that corona formation preceded major extension also exists (Stofan *et al.* 1993, Hamilton and Stofan 1994). These relationships indicate that under some circumstances, extension may influence the placement and concentration of coronae, and under others, coronae may influence the surface expression and concentration of extensional stresses. Baer *et al.* (1994) examined the relationship between coronae and extensional belts in northern Lada Terra and found evidence of similar relationships between fractures and coronae. These coeval relationships indicate that the extensional and corona-forming processes in these environments are closely connected and suggest that neither process dominates or consistently precedes the other.

*Corona formation and Rayleigh–Taylor instabilities.* The spacing of upwelling diapirs (forming coronae) may

reflect the presence of a Rayleigh–Taylor-type instability in the upper mantle, with corona formation directed along zones of thermal weakness in the lithosphere. Initial calculations for establishing the depth of corona origination, based on the existence of a Rayleigh–Taylor instability at depth, indicate that the source region of these features is between approximately 150 and 200 km in the Hecate Chasma area. Plumes from these depths could produce not just coronae, but also shallow magma bodies locally extruding with the aid of regional extension. Terrestrial models of Rayleigh–Taylor instabilities suggest that at spreading centers, mantle uplift results in decompression melting, and the melt ascends to the crust due to its lower density compared to that of the crust (Whitehead *et al.* 1984). It is possible that a zone of partial melting exists at depths from 150–200 km in the Hecate Chasma region and is responsible for the formation of diapirs resulting in corona formation. A chemical boundary at these depths seems unlikely, as mantle compositions are generally assumed to become more dense with depth. It is entirely possible that coronae in zones of concentrated deformation, including Hecate Chasma, are due to processes other than Rayleigh–Taylor instabilities. At this time, there is not enough geophysical evidence to prove or disprove the existence of these instabilities; we simply speculate as to what information such a model provides about the origins of coronae in this region.

After comparing the observed features with a model of subduction/delamination and an extensional model, we find that the predominance of features related to extension and upwelling implies that the tectonic features of this region are the result of lithospheric extension with limited rifting. Continuing studies examine a trough and corona chain along Parga Chasma and evaluate the relationship between Hecate Chasma and Parga Chasma, as well as the associations of these corona chains and deformational zones to major hotspots such as Beta, Atla, and Themis Regions.

## ACKNOWLEDGMENTS

The authors thank D. M. Janes, R. E. Grimm, M. H. Bulmer, and an anonymous reviewer for careful reviews of the manuscript and helpful suggestions. This research was carried out at Arizona State University and the Jet Propulsion Laboratory under a National Physical Science Consortium Graduate Fellowship and National Aeronautics and Space Administration Grant NAS-151-0101-70-59.

## REFERENCES

- BAER, G., G. SCHUBERT, D. L. BINDSCHADLER, and E. R. STOFAN 1994. Spatial and temporal relations between coronae and extensional belts, northern Lada Terra, Venus. *J. Geophys. Res.* **99**, 8355–8369.
- BARSUKOV, V. L., A. T. BASILEVSKY, G. A. BURBA, N. N. BOBINA, B. P. KRYUCHKOV, R. O. KUZMIN, O. N. NIKOAEVA, A. A. PRONIN, L. B. RONCA, I. M. CHERNAYA, V. P. SHASHKINA, A. V. GARANIN,

- E. R. KUSHKY, M. S. MARKOV, A. L. SUKHANOV, V. A. KOTELNIKOV, O. N. RZHIGA, G. M. PETROV, YU. N. ALEXANDROV, A. I. SIDORENKO, A. F. BOGOMOLOB, G. I. SKRYPNIK, M. YU. BERGMAN, L. V. KUDRIN, I. M. BOKSHEIN, M. A. KRONROD, P. A. CHOCHIA, YU. S. TYUFLIN, S. A. KADNICHANSKY, AND E. L. AKIM 1986. The geology and geomorphology of the Venus surface as revealed by the radar images obtained by Veneras 15 and 16. *J. Geophys. Res.* **91**, 378–398.
- BINDSCHADLER, D. L., G. SCHUBERT, AND W. M. KAULA 1992. Coldspots and hotspots: Global tectonics and mantle dynamics of Venus. *J. Geophys. Res.* **97**, 13,495–13,532.
- BIOT, M. A. AND H. ODÉ 1965. Theory of gravity instability with variable overburden and compaction. *Geophysics* **30**, 213–227.
- BONATTI, E. 1985. Punctiform initiation of seafloor spreading in the Red Sea during transition from a continental to an oceanic rift. *Nature*, **316**, 33–37.
- BROWN, C. D., AND R. E. GRIMM 1995. Tectonics of Artemis chasma: A venusian “plate” boundary. *Icarus*. **117**, 219–249.
- CRANE, K. 1985. The spacing of rift axis highs: Dependence upon diapiric processes in the underlying asthenosphere?. *Earth Planet. Sci. Lett.* **72**, 405–414.
- GRIMM, R. E. AND R. J. PHILLIPS 1992. Anatomy of a venusian hot spot: Geology, gravity, and mantle dynamics of Eistla Regio. *J. Geophys. Res.* **97**, 16,035–16,054.
- GRIMM, R. E., AND S. C. SOLOMON 1987. Limits on modes of lithospheric heat transport on Venus from impact crater density. *Geophys. Res. Lett.* **14**, 538–541.
- HAMILTON, V. E. AND E. R. STOFAN 1993. Morphology and models for the evolution of eastern Hecate Chasma, Venus, *Lunar Planet. Sci.* **XXIV**, 597. [Abstract]
- HAMILTON, V. E. AND E. R. STOFAN 1994. The geology and evolution of Hecate Chasma, Venus. *Lunar Planet. Sci.* **XXV**, 501. [Abstract]
- HANSEN, V. L., AND R. J. PHILLIPS 1993. Tectonics and volcanism of Eastern Aphrodite Terra, Venus: No subduction, no spreading. *Science*, **260**, 526–530.
- HEAD, J. W., L. S. CRUMPLER, J. C. AUBELE, J. E. GUEST, AND R. S. SAUNDERS 1992. Venus volcanism: Classification of volcanic features and structures, association, and global distribution from Magellan data. *J. Geophys. Res.* **13**, 153–197.
- HERRICK, R. R., AND R. J. PHILLIPS 1992. Geological correlations with the interior density structure of Venus. *J. Geophys. Res.* **97**, 16,017–16,034.
- JANES, D. M., S. W. SQUYRES, D. L. BINDSCHADLER, G. BAER, G. SCHUBERT, V. L. SHARPTON, AND E. R. STOFAN 1992. Geophysical models for the formation and evolution of coronae on Venus. *J. Geophys. Res.* **97**, 16,055–16,067.
- KOCH, D. M. 1994. A spreading drop model for plumes on Venus. *J. Geophys. Res.* **99**, 2035–2052.
- LEWIS, B. T. R. 1981. Isostasy, magma chambers and plate driving forces on the East Pacific Rise. *J. Geophys. Res.* **86**, 4868–4880.
- LUCCHITA, B. K. 1977. Topography, structure, and mare ridges in southern Mare Imbrium and northern Oceanus Procellarum. *Proc. Lunar Sci. Conf.* **8**, 2691–2703.
- MASURSKY, H., E. ELIASON, P. G. FORD, G. E. MCGILL, G. H. PETTENGILL, G. G. SCHABER, AND G. SCHUBERT 1980. Pioneer Venus radar results: Geology from images and altimetry. *J. Geophys. Res.* **85**, 8232–8260.
- MAXWELL, T. A., F. EL-BAZ, AND S. H. WARD, 1975. Distribution, morphology, and origin of ridges and arches in Mare Serenitatis. *Geol. Soc. Amer. Bull.* **86**, 1273–1278.
- MCGILL, G. E., S. J. STEENSTRUP, C. BARTON, AND P. G. FORD 1981. Continental rifting and the origin of Beta Regio. *Geophys. Res. Lett.* **8**, 737–740.
- MCKENZIE, D., P. G. FORD, C. JOHNSON, B. PARSONS, D. SANDWELL, S. SAUNDERS, AND S. C. SOLOMON 1992. Features on Venus generated by plate boundary processes. *J. Geophys. Res.* **97**, 13,533–13,544.
- PHILLIPS, R. J. 1994. Estimating lithospheric properties at Atla Regio, Venus. *Icarus* **112**, 147–170.
- PRONIN, A. A., AND E. R. STOFAN 1990. Coronae on Venus: Morphology and distribution. *Icarus* **87**, 452–474.
- RABINOWICZ, M., A. NICOLAS, AND J. L. VIGNERESSE 1984. A rolling mill effect in asthenosphere beneath oceanic spreading centers. *Earth Planet. Sci. Lett.* **67**, 97–108.
- ROBERTS, K. M., J. E. GUEST, J. W. HEAD, AND M. G. LANCASTER 1992. Mylitta Fluctus, Venus: Rift-related, centralized volcanism and the emplacement of large-volume flow units. *J. Geophys. Res.* **97**, 15,991–16,015.
- SANDWELL, D. T. AND G. SCHUBERT 1992a. Evidence for retrograde lithospheric subduction on Venus. *Science* **257**, 766–770.
- SANDWELL, D. T. AND G. SCHUBERT 1992b. Flexural ridges, trenches, and outer rises around coronae on Venus. *J. Geophys. Res.* **97**, 16,069–16,083.
- SCHABER, G. G. 1982. Venus: Limited extension and volcanism along zones of lithospheric weakness. *Geophys. Res. Lett.* **9**, 499–502.
- SCHOUTEN, H., K. D. KLITGORD, AND J. A. WHITEHEAD 1985. Segmentation of mid-ocean ridges. *Nature* **317**, 225–229.
- SCHUBERT, G., AND D. T. SANDWELL 1995. A global survey of possible subduction sites on Venus. *Icarus* **117**, 173–139.
- SCHUBERT, G., D. BERCOVICI, AND G. A. GLATZMAIER 1990. Mantle dynamics in Mars and Venus: Influence of an immobile lithosphere on three-dimensional mantle convection. *J. Geophys. Res.* **95**, 14,105–14,129.
- SENSKE, D. A. 1990. Geology of the Venus equatorial region from Pioneer Venus radar imaging. *Earth, Moon and Planets.* **50/51**, 305–327.
- SENSKE, D. A., D. B. CAMPBELL, E. R. STOFAN, P. C. FISHER, J. W. HEAD, N. STACY, J. C. AUBELE, A. A. HINE, AND J. K. HARMON 1991a. Geology and tectonics of Beta Regio, Guinevere Planitia, Sedna Planitia, and Western Eistla Regio, Venus: Results from Arecibo image data. *Earth, Moon and Planet.* **55**, 163–214.
- SENSKE, D. A., J. W. HEAD, E. R. STOFAN, AND D. B. CAMPBELL 1991b. Geology and structure of Beta Regio, Venus: Results from Arecibo radar imaging. *Geophys. Res. Lett.* **18**, 1159–1162.
- SENSKE, D. A., G. G. SCHABER, AND E. R. STOFAN 1992. Regional topographic rises on Venus: Geology of Western Eistla Regio and comparison to Beta Regio and Atla Regio. *J. Geophys. Res.* **97**, 13,395–13,420.
- SMREKAR S. E., AND R. J. PHILLIPS 1991. Venusian highlands: Geoid to topography ratios and their implications. *Earth Planet. Sci. Lett.* **107**, 582–597.
- SOLOMON, S. C. AND J. W. HEAD 1982. Mechanisms for lithospheric heat transport on Venus: Implications for tectonic style and volcanism. *J. Geophys. Res.* **87**, 9,236–9,246.
- SQUYRES, S. W., D. M. JANES, G. BAER, D. L. BINDSCHADLER, G. SCHUBERT, V. L. SHARPTON, AND E. R. STOFAN 1992. The morphology and evolution of coronae and novae on Venus. *J. Geophys. Res.* **97**, 13,611–13,634.
- STOFAN, E. R., D. L. BINDSCHADLER, J. W. HEAD, AND E. M. PARMENTIER 1987. Corona structures on Venus: Models of origin. *Lunar Planet. Sci.* **XXVIII**, 954–955. [Abstract]
- STOFAN, E. R., AND J. W. HEAD 1990. Coronae of Mnemosyne Regio, Venus: Morphology and origin. *Icarus* **83**, 216–243.
- STOFAN, E. R., J. W. HEAD, AND D. B. CAMPBELL 1990. Beta-Eistla deformation zone: Analysis from recent Arecibo radar images. *Lunar Planet. Sci.* **XXI**, 1208–1209. [Abstract]

- STOFAN, E. R., D. L., BINDSCHADLER, J. W. HEAD, AND E. M. PARMENTIER 1991. Coronae on Venus: Models of origin. *J. Geophys. Res.* **96**, 20,933–20,946.
- STOFAN, E. R., V. L. SHARPTON, G. SCHUBERT, G. BAER, D. L. BINDSCHADLER, D. M. JANES, AND S. W. SQUYRES 1992. Global distribution and characteristics of coronae and related features on Venus: Implications for origin and relation to mantle processes. *J. Geophys. Res.* **97**, 13,347–13,378.
- STOFAN, E. R. 1993. Corona annuli: Characteristics and modes of origin. *Eos, Trans. AGU* **74**, 377. [Abstract]
- STOFAN, E. R., V. E. HAMILTON, AND K. COTUGNO 1993. Parga and Hecate Chasmata, Venus: Structure, volcanism and models of formation. *Lunar Planet. Sci.* **XXIV**, 1361–1362. [Abstract]
- STOFAN, E. R., S. E. SMREKAR, D. L. BINDSCHADLER, AND D. A. SENSKE 1995. Large topographic rises on Venus: Implications for mantle upwelling. *J. Geophys. Res.* **100**, 23,317–23,327.
- TACKLEY, P. J., AND D. J. STEVENSON 1991. The production of small venusian coronae by Rayleigh-Taylor instabilities in the uppermost mantle. *Eos, Trans. AGU* **72**, 287. [Abstract]
- TACKLEY, P. J., D. J. STEVENSON, AND D. R. SCOTT 1992. Volcanism by melt-driven Rayleigh–Taylor instabilities and possible consequences of melting for admittance ratios on Venus. In *Papers Presented to the International Colloquium on Venus, Lunar Planet. Inst. Contrib.* 789, pp. 123–124, Lunar and Planetary Institute, Houston, Texas. [Abstract]
- TURCOTTE, D. L. AND G. SCHUBERT 1982. *Geodynamics: Applications of Continuum Physics to Geological Problems*. Wiley, New York.
- VENING MEINESZ, F. A. 1950. Les “graben” africains résultat de compression ou de tension dans la croûte terrestre? *K. Belg. Kol. Inst. Bull.* **21**, 539–552.
- WATTERS, T. R. AND T. A. MAXWELL 1986. Orientation, relative age, and extent of the Tharsis plateau ridge system. *J. Geophys. Res.* **91**, 8113–8125.
- WHITEHEAD, J. A., H. J. B. DICK, AND H. SCHOUTEN 1984. A mechanism for magmatic accretion under spreading centers. *Nature* **312**, 146–148.
- ZUBER, M. T. 1987. Constraints on the lithospheric structure of Venus from mechanical models and tectonic surface features. *J. Geophys. Res.* **92**, E541–E551.
- ZUBER, M. T., E. M. PARMENTIER, AND R. C. FLETCHER 1986. Extension of continental lithosphere: A model for two scales of basin and range deformation. *J. Geophys. Res.* **91**, 4826–4838.